Research Square

Preprints are preliminary reports that have not undergone peer review.
They should not be considered conclusive, used to inform clinical practice,
or referenced by the media as validated information.

Morphological and transcriptomic dynamics of flower development in Phyllostachys reticulata

Yonglong Li
Forestry College, Jiangxi Agricultural University
Xujie Huang
Forestry College, Jiangxi Agricultural University
Heng Liu
Forestry College, Jiangxi Agricultural University
Chengkun Wang
Forestry College, Jiangxi Agricultural University
Jiajing Peng
Forestry College, Jiangxi Agricultural University
Wengen Zhang
Forestry College, Jiangxi Agricultural University
Chunce Guo
Forestry College, Jiangxi Agricultural University
Meixia Wang
meixiawang@jxau.edu.cn

Forestry College, Jiangxi Agricultural University

Research Article

Keywords: Phyllostachys reticulata, flower development, floral organogenesis, male and female gametophyte development, MADS-box genes

Posted Date: November 10th, 2026

DOI: https://doi.org/10.21203/rs.3.rs-11459276/v1

License: This work is licensed under a Creative Commons Attribution 4.0 International License.
Read Full License

Additional Declarations: No competing interests reported.

Abstract

Background

The prolonged and often unpredictable flowering cycles of bamboos have limited studies of their reproductive development. In *Phyllostachys reticulata*, the relationships among inflorescence organization, floral organogenesis, gametophyte development, and tissue-specific transcriptional programs remain unclear. We combined morphological observations, serial histological sections, and PacBio and Illumina transcriptome sequencing to characterize floral development, establish a reference transcriptome resource, and identify candidate regulators.

Results

Morphological and histological observations revealed distinct spatial patterns of floret initiation and maturation. Floret primordia were initiated sequentially from the apex toward the base of the spikelet, whereas basal florets developed faster than apical florets. Floral organs differentiated centripetally, successively forming the lemma, palea, lodicules, stamens, and carpel. Male gametophyte development culminated in bicellular pollen, with collapsed pollen grains occurring alongside well-developed pollen in mature anthers. Female development produced seven-celled, eight-nucleate Polygonum-type embryo sacs. Integration of PacBio long-read and Illumina short-read sequencing generated a reference transcriptome comprising 259,726 non-redundant protein-coding sequences. Expression analysis identified 33,765 differentially expressed transcripts among six tissue types, with lemmas and paleae exhibiting the most similar expression profiles. Co-expression analysis identified modules associated with leaves, outer floral organs, stamens, and carpels. Thirty-eight candidate ABCDE(G)-class MADS-box transcripts exhibited divergent tissue-associated expression patterns. Homologs of established flowering regulators differed in expression between leaves from flowering and non-flowering branches, encompassing photoperiodic signaling, florigen-associated pathways, and floral meristem identity regulation.

Conclusions

This study establishes an integrated morphological and transcriptional framework for floral development in *P. reticulata*, distinguishing spatial developmental patterns and identifying candidate transcriptional programs associated with flowering status and floral organ differentiation. The reference transcriptome provides a sequence resource for investigating reproduction in this species and comparing conservation and divergence in bamboo floral development. Future functional studies could clarify the roles of key candidates in floral development and seed formation.

Background

Bamboos are important forest and renewable biomass resources that play essential roles in wood substitution, ecological environment maintenance, and the supply of bamboo timber and shoots [1, 2]. Their flowering and reproductive development are directly associated with sexual reproduction, population renewal, and the sustainable utilization of bamboo resources. The reproductive processes including the vegetative-to-reproductive phase transition, the initiation and differentiation of inflorescences and floral organs, male and female gametophyte development, fertilization and seed formation, collectively determine the successful completion of reproduction [3]. Accordingly, a systematic characterization of bamboo flowering and reproductive development is essential not only for elucidating the distinctive life-history strategies of bamboos, but also for assessing the consequences of flowering for bamboo forest regeneration and resource stability.

Bamboo flowering and reproductive development display pronounced temporal, spatial, and structural heterogeneity. The vegetative phase varies among species from several years to multiple decades or even more than a century. Within a single species, flowering may occur sporadically, locally, or synchronously across large populations. Following flowering and seed production, a clone may undergo post-reproductive senescence and die, or persist through the continued survival of non-flowering ramets [1, 4, 5]. Although more than 1,600 bamboo species have been identified worldwide, comprehensive floral morphological information is available for only a small proportion of them. Flowering records have been reported for approximately 265 species, whereas detailed descriptions of floral morphology exist for only about 45 species, severely constraining investigations into bamboo floral diversity and its developmental determinants [5, 6]. Published studies are likewise concentrated on a limited number of taxa and frequently focus only on mature inflorescences, individual floral organs, or discrete stages of gametophyte development. Continuous developmental evidence encompassing inflorescence initiation, spikelet and floret differentiation, and the formation of male and female gametophytes remains limited. The long flowering cycles, unpredictable flowering time, rapid post-anthesis degradation of reproductive materials, and difficulty in obtaining fertile specimens further impede in-depth analyses of bamboo floral diversity and its underlying developmental mechanisms. Therefore, it is essential to obtain materials from consecutive developmental stages and conduct morphological observations, histocytological examinations, and transcriptome expression analyses.

A particularly remarkable reproductive characteristic of bamboos is the exceptionally prolonged flowering periodicity, ranging from several decades to more than a century. Moreover, clonally related populations separated by substantial geographic distances may undergo flowering with near synchrony. Various hypotheses have been proposed to explain this phenomenon, including a genetically controlled endogenous biological clock, physiological resource accumulation, environmentally induced flowering, predator satiation, and the fire-cycle hypothesis. Nevertheless, no single hypothesis adequately explains the full developmental stages of bamboo flowering periodicity, spatial synchronisation and interspecific variation [1, 4, 5, 7]. From an evolutionary-developmental perspective, flowering time is determined by regulatory processes governing the developmental transition from vegetative to reproductive growth. Research in model plants has demonstrated that signaling pathways responsive to photoperiod, temperature, vernalization, phytohormones and endogenous developmental cues ultimately converge on

floral integrators such as FT and SOC1, as well as downstream floral meristem identity genes, collectively determining the initiation of floral transition. Distinct plant lineages may evolve divergent flowering responses through gene duplication and loss, functional diversification among homologous genes and rewiring of regulatory interactions [8–10]. This conceptual framework derived from model plants provides an essential foundation for identifying evolutionarily conserved regulatory nodes in bamboos, assessing functional divergence among homologous family members and reconstructing candidate flowering-regulatory networks.

Evidence from transcriptomic studies of moso bamboo (*Phyllostachys edulis*), *Dendrocalamus latiflorus*, and *Bambusa oldhamii* 'Xia Zao' suggests that floral transition in bamboos involves multiple regulatory pathways rather than a single locus [11–13]. Studies of FT homologues and photoperiod-associated genes have identified key, though likely incomplete, candidates connecting environmental signals with floral transition [14–16]. Functional characterization of the SOC1-like gene BoMADS50 has provided evidence for a role in floral transition in *B. oldhamii* [17]. Other studies have examined Dof transcription factors in floral development and stress responses [18, 19], SVP-like regulators [20, 21], and small RNAs associated with flower formation and development [11]. These findings support a broadly conserved flowering-regulatory framework while revealing variation among genes, tissues, and species. However, much of the available evidence derives from homology-based annotation, correlative expression analyses, or heterologous functional assays. Floral-state-associated transcriptomic changes and candidate regulatory networks therefore need to be characterized in additional bamboo taxa to distinguish shared components from lineage-specific regulatory features.

Bamboo inflorescences are fundamentally organized into spikelets or pseudospikelets, consistent with the canonical architectural framework of Poaceae. The floral organ whorls are consistently initiated centripetally from the periphery toward the center, in the sequential order of lemma, palea, lodicules, stamens, and pistil. However, substantial interspecific variation exists in inflorescence branching architecture, spikelet organization, floret number per spikelet, and the number and morphology of bracts, glumes, lemmas, paleas, lodicules, stamens, and pistils [6, 22, 23]. Based on developmental processes, floral transition merely marks the onset of reproductive development and is followed by organ primordium initiation, organ identity specification, morphogenesis, and maturation. Whereas cell identity specification determines the developmental fate of an organ, morphogenesis defines its ultimate dimensions, geometry, and histological organization through coordinated cell proliferation, expansion, differentiation, and the establishment of organ polarity [24]. The ABCDE(G) framework posits that A-class (FUL-like), B-class (AP3/PI-like), C-class (AG-like), D-class (STK/AGL11-like), E-class (SEP-like), and G-class (AGL6-like) MADS-box transcription factors act combinatorially to specify floral meristem identity and the identities of floral whorl organs. In Poaceae, *AGL6-like* genes additionally contribute to palea and pistil development and to the maintenance of floral meristem determinacy [25–28]. Homologues representing these functional classes have been characterized in bamboos. In *P. praecox*, *PpMADS1* and *PpMADS2* are implicated in floral transition [29]. Functional evidence is also available for the bamboo MADS-box gene BeMADS1 in Bambusa edulis [30]. Furthermore, gene family analyses and transcriptomic profiling support putative roles for MADS-box genes in floral development in *P. edulis* and

Dendrocalamus latiflorus [11, 31, 32]. Nevertheless, floral organ identity genes account for only one component of organ development; following primordium establishment, cell-cycle regulation, cell-wall remodeling, phytohormone signaling, and tissue differentiation collectively shape organ morphology and reproductive competence. Although defective anther ontogeny, reduced pollen viability, and low seed-set rates have been documented in bamboos, existing investigations remain predominantly descriptive at the morphological and anatomical levels and have yet to establish mechanistic relationships between these phenotypic abnormalities and specific regulatory pathways [33, 34]. Accordingly, research on bamboo flowers needs to move beyond the mere identification of identity genes toward an integrated analysis of inflorescence architecture, organogenesis, gametophyte development, and tissue-level expression programs.

Phyllostachys reticulata is a large, monopodial bamboo species indigenous to China. Its widespread distribution across China renders it one of the most economically significant bamboo taxa. Compared with moso bamboo, *P. reticulata* exhibits greater cold tolerance and consequently extends farther north in its natural distribution. It is widely distributed throughout the Yellow River basin and regions farther south, with wild populations occurring from the Wuyi Mountains westward through the Nanling Mountains to southwestern China. Its robust and rigid culms are extensively used in construction, flooring, furniture manufacture, and weaving. Furthermore, its sweet, edible shoots confer additional value as a food resource. Thus, *P. reticulata* is cultivated as a dual-purpose species for both culm and shoot production. Cultivars with variations in culm color or internode morphology, such as *P. reticulata* 'Jinming', also possess considerable ornamental value in landscaping [35–37].

Previous investigations have described floral bud initiation, flowering phenology, inflorescence architecture, pollen germinability, and natural seed production in *P. reticulata*, and have revealed phenomena such as staggered flowering within the same bamboo forest, relatively low pollen germination rates, and sparse natural seed set [38]. *P. reticulata* is closely related to moso bamboo (*P. edulis*) within the same genus, which currently represents one of the most extensively studied bamboo species with respect to floral ontogeny and the molecular regulation of flowering. Despite their close relationship, however, the two species exhibit pronounced differences in reproductive morphology. In *P. reticulata*, the flowering branches are spicate, with spikelets developing in the axils of spathaceous bracts, and each spikelet generally comprises one to three florets and either lacks glumes or bears a single glume. Moso bamboo also has a complex spikelet system [22], and its spikelets have been reported to contain 1–6 florets and 1–3 glumes [39]. These interspecific differences in inflorescence organization, floret number, and glume complement render the two taxa particularly suitable for comparative analyses of the conserved developmental programs operating within *Phyllostachys* and the ontogenetic mechanisms underlying species-specific floral architectures. Nevertheless, floral organ development and associated transcriptional regulatory networks remain largely unexplored in *P. reticulata*.

In this study, paraffin-embedded histological analyses of floral organs across multiple developmental stages revealed the distinct developmental dynamics of inflorescence differentiation, spikelet initiation,

floral organogenesis, and male and female gametophyte development in *P. reticulata*, together with their associated anatomical differences. Phylogenetic analysis identified 38 candidate ABCDE(G)-class MADS-box transcripts, whose expression profiles were examined across six tissues. Weighted gene co-expression network analysis (WGCNA) separately identified organ-associated modules, providing complementary candidates for investigating floral development in *P. reticulata*. Collectively, the integration of morphological and anatomical characterization with tissue-specific gene-expression profiling would provide a systematic framework for elucidating the complete reproductive developmental trajectory of *P. reticulata*.

Methods

Plant material and sample collection

Plant material of *P. reticulata* was collected from the bamboo garden of Jiangxi Agricultural University, and voucher specimens were deposited in the Herbarium of Jiangxi Agricultural University (JXAU). The inflorescences with no visible signs of pest infestation or disease were collected during the flowering stage. We recorded the growth and morphological changes from floral bud initiation to inflorescence maturation. Thirty fully developed and mature inflorescences were selected and sequentially dissected under a stereomicroscope (Stemi 2000-C; Carl Zeiss, Germany). The number of inflorescence-axis nodes, characteristics of bract, positions of spikelets, the number of florets, and the number and morphology of lemmas, paleae, lodicules, stamens, and pistils were also recorded. Additionally, 10 well-developed inflorescences were selected to quantify the numbers of latent buds and spikelets. Floret numbers were determined separately for the terminal spikelet and the most fully developed lateral spikelet within each inflorescence. All data were expressed as mean ± standard deviation (SD).

RNA sequencing was performed using seven tissue types: leaves from non-flowering branches (Nfl), leaves from flowering branches (Fl), lemmas (Le), paleae (Pa), lodicules (Lo), stamens (St), and carpels (Ca), with four biological replicates per tissue for Illumina sequencing. Lodicule libraries were generated and sequenced but were excluded from the downstream differential-expression and co-expression analyses because of poor within-group clustering. Three biological replicates from each of the remaining six tissues were retained after sample-level quality assessment, as detailed in the Results subsection on transcriptome sequencing and sample quality assessment. Following dissection, all tissue samples were immediately flash-frozen in liquid nitrogen and stored at -80°C.

Morphological and histological observations

Inflorescences, spikelets, and florets at different developmental stages were collected for paraffin sectioning and immediately immersed in 50% FAA solution. The samples were subsequently transferred to 70% FAA, and were vacuum-infiltrated again, and fixed for at least 48 hours. All samples were dehydrated through a graded ethanol series of 50%, 70%, 85%, 95%, and 100%, followed by clearing in

ethanol:xylene mixtures at volume ratios of 3:1, 1:1, and 1:3. After clearing, the samples were infiltrated with paraffin buffer at 65°C.

All samples were embedded in paraffin solutions at 75°C using a KD-BM embedding system. Serial sections (8 μm thick) were prepared using a Leica RM2235 rotary microtome, mounted on glass slides, and incubated at 38°C for 3–7 days. Following rehydration, the sections were stained with safranin for 24 hours and counterstained with Fast Green for 15–30 s. Microscopic examination and image acquisition were performed using a Zeiss AX10 microscope.

RNA-seq library construction and sequencing

The collected samples were sent to Novogene Co., Ltd. (Beijing, China) for transcriptome library preparation and sequencing. For PacBio sequencing, equal amounts of total RNA derived from three biological replicates of each tissue were used to construct a full-length transcriptome library. Single-molecule real-time (SMRT) sequencing was performed on the PacBio Sequel platform [40].

In parallel, four biological replicates of the Nfl, Fl, Le, Pa, Lo, St, and Ca samples were used to prepare Illumina RNA-seq libraries, followed by 150-bp paired-end sequencing on the Illumina HiSeq 2500 platform (Table S1). The raw reads were processed using fastp software (version 0.18.0) to remove adapter reads, reads containing ambiguous nucleotides, and low-quality reads [41]. Following quality assessment based on sequencing metrics, principal component analysis (PCA), and intersample correlation analysis, 18 high-quality Illumina libraries were finally retained for differential-expression and co-expression analyses.

Construction of the reference transcriptome

PacBio raw reads were processed using SMRT Link v8.0 with the following parameter settings: minLength 50, maxLength 15000, and minPasses 1. Error-corrected reads were initially generated using the circular consensus sequencing (CCS) algorithm. Full-length non-chimeric (FLNC) and non-full-length non-chimeric reads were subsequently classified based on the presence of 5' and 3' primer sequences and poly(A) tails. The FLNC reads were clustered using the hierarchical n*log(n) algorithm, followed by consensus polishing to generate high-quality transcript isoforms. These consensus sequences were further corrected with LoRDEC using Illumina clean reads [42].

Illumina short reads were independently *de novo* assembled using Trinity software [43, 44]. The resulting Trinity-assembled transcripts were combined with the PacBio-derived transcripts and subjected to CD-HIT clustering at 95% sequence identity [45]. Open reading frames (ORFs) were predicted using TransDecoder v5.5.0 [44]. Candidate peptide sequences were aligned against UniProt and protein databases from phylogenetically related species using DIAMOND (v2.1.9.163) with an E-value cutoff of 1×10^{-5} [46]. Conserved protein domains were identified against Pfam-A v34.0 using the hmmsearch module implemented in HMMER (v3.4), with an E-value threshold of 1×10^{-5} [47, 48]. Homology- and

domain-based evidence was incorporated into coding-sequence prediction using TransDecoder.Predict with the retain_blastp_hits and retain_pfam_hits options. The predicted coding sequences were subsequently subjected to a second CD-HIT clustering step at 95% sequence identity, and the representative sequence identifiers were mapped back to their corresponding Trinity or PacBio transcripts to construct the final non-redundant protein-coding reference dataset. Dataset completeness was assessed in protein mode using BUSCO v5.7.1 against the embryophyta_odb10 and poales_odb10 lineage-specific datasets [49].

Transcript quantification and differential-expression and co-expression analyses

Quality-filtered clean reads from the 18 Illumina libraries were mapped to the final non-redundant reference transcriptome using Salmon, generating raw count and TPM expression matrices [50]. The 5,000 transcripts exhibiting the highest expression variance were selected, and their TPM values were transformed as $\log_2$ (TPM + 1) prior to PCA analysis. Differential expression analysis was performed using DESeq2 [51]. Transcripts with fewer than 10 cumulative counts across all samples were excluded, and all 15 pairwise contrasts among the six tissues were evaluated. Size factors and dispersion parameters were estimated directly from the raw-count matrix, and differential expression was assessed using Wald tests. Transcripts with both a Benjamini–Hochberg-adjusted *P* value (padj) < 0.01 and an absolute $\log_2$ fold change ($|\log_2 FC|$) ≥ 4 were classified as significantly differentially expressed. UpSet plots were subsequently generated to delineate shared and comparison-specific differentially expressed transcripts across the 15 pairwise contrasts.

Weighted gene co-expression network analysis was performed using WGCNA v1.72.5. Transcripts with TPM ≥ 1.0 in at least 30% of the samples were retained, and the expression matrix was $\log_2$(TPM + 1)-transformed [52]. The top 5,000 transcripts with the highest median absolute deviation (MAD) were selected to construct a signed co-expression network. Modules were merged using a module eigengene dissimilarity threshold of 0.25. Pearson correlation coefficients and corresponding *P* values were calculated between module eigengenes (MEs) and the traits Nfl, Fl, Le, Pa, St, Ca, as well as their combinations. Candidate hub genes were prioritized by integrating module membership (MM), gene significance (GS) for the corresponding traits, and intramodular connectivity. The 200 genes with the highest intramodular connectivity were retained, and the leading hub genes were visualized using Cytoscape v3.10.1 [53].

Functional enrichment analysis

All transcripts of *P. reticulata* were subjected to homology searches against the MapMan database, and significant matches were retained at *P* < 0.05. Functional annotations were assigned to the *P. reticulata* transcripts based on these matches, and a TERM2GENE mapping table linking functional categories to their corresponding genes was subsequently generated. Functional enrichment analyses were

conducted independently for differentially expressed gene sets and genes assigned to target WGCNA modules using the enricher function in the clusterProfiler package [54]. All genes with MapMan annotations in the annotation file were used as the background gene set. The *P* values of enrichment were adjusted for multiple comparisons using the Benjamini–Hochberg procedure (Tables S2). Enrichment bubble plots were generated using ggplot2 software, with bubble size indicating the number of genes assigned to each functional term and color representing $-\log_{10}$ (*P* value), thereby facilitating comparisons of the predominant functional profiles and enrichment magnitudes among co-expression modules (Tables S3–S7).

Flowering regulatory network and identification of ABCDE(G)-class MADS-box candidates

Flowering regulatory network nodes were curated from previously characterized processes including photoperiodic and circadian regulation, photoperiodic signal integration, florigen transport, and floral meristem identity in model plant species [55–60]. Using rice proteins as references, candidate homologous sequences in *P. reticulata* were identified through homologous sequence clustering and phylogenetic reconstruction based on protein datasets from rice (*Oryza sativa*), moso bamboo (*P. edulis*), and *P. reticulata*. Accordingly, a single rice network node could be represented by multiple candidate transcripts in *P. reticulata*.

Annotated rice MADS-box proteins were used as references to identify putative class A, B, C, D, E and G members in *P. reticulata*. Multiple sequence alignment of 96 proteins from rice, moso bamboo, and *P. reticulata* was conducted using MAFFT v7 [61], followed by the removal of poorly aligned sites with trimAl -gt 0.20 [62]. The JTT+G4 algorithm was chosen to construct the maximum-likelihood based phylogenetic tree via IQ-TREE 2 software. Branch support was assessed using 1,000 ultrafast bootstrap replicates and 1,000 SH-aLRT replicates [63]. ABCDE(G) functional classes were assigned according to the phylogenetic placement of candidate proteins. For each MADS-box subclass, Friedman tests were performed using transcript-level $\log_2$ (mean TPM + 1) values across the six tissues as paired observations. The resulting *P* values for the six subclasses were corrected for multiple testing using the Benjamini–Hochberg procedure.

Results

Flowering and morphology of inflorescences, spikelets, and florets

To characterize the flowering process and hierarchical organization of inflorescences, spikelets, and florets of *P. reticulata*, we performed continuous phenological monitoring and morphological dissections of mature inflorescences. Flowering occurred predominantly sporadically and was observed mainly in normal and mature culms, although direct flowering on newly emerged culms and bamboo shoots was

also observed. Throughout the observation period, flowering individuals and their associated rhizomes maintained active growth, with no evident whole-plant mortality following anthesis. Moreover, no fully developed caryopses were detected in mature inflorescences, indicating a low natural seed-set rate (Supplementary Fig. 1). Flowering branches exhibited a three-tiered branching architecture comprising primary, secondary, and tertiary axes. Anthesis progressed sequentially along the tertiary flowering branches from the distal nodes toward the basal nodes. (Fig. 1A). From floral-bud differentiation to mature-inflorescence formation, *P. reticulata* morphology underwent a series of successive developmental transitions (Fig. 1B). The mature inflorescence consisted of a multinodal inflorescence axis, with spikelet-like units arising from the axils of bracts at each node. However, the developmental states of both bracts and spikelets varied substantially among nodes (Fig. 1C). Collectively, these findings demonstrated that sporadically flowering *P. reticulata* retained vegetative growth competence and that inflorescence anthesis followed a clear directional pattern, progressing from the upper nodes toward the base along the tertiary flowering branches.

Unlike the basipetal anthesis of inflorescences along the flowering branches, spikelet ontogeny on the inflorescence axis generally proceeded acropetally, although developmental competence did not exhibit a strictly linear nodal progression. Spikelets at the basal two to three nodes typically underwent developmental arrest and persisted as latent buds, whereas those at the middle and upper nodes attained the greatest degree of differentiation. Toward the apex, spikelet development became comparatively delayed again. With the exception of the bracts subtending the terminal spikelet, the outer bracts associated with the median and upper lateral spikelets were conspicuously enlarged and differentiated into spathes. Quantitative assessment of 10 intact inflorescences revealed that each inflorescence comprised 4–8 spikelet or latent-buds, including 3–5 actively developing spikelets and 1–3 developmentally arrested (Supplementary Fig. 2A). The terminal spikelet lacked a prophyll and was enclosed by bracts inserted at the apex of the inflorescence axis. By contrast, each lateral spikelet possessed a prophyll approximately 1–1.5 cm long, positioned between the spathe bract and the first glume (Fig. 1D - E). Furthermore, its internal organization was essentially congruent with that of the terminal spikelet (Fig. 1D - E). Collectively, these observations demonstrated a distinct developmental program along the inflorescence axis, characterized by developmental arrest at the basal nodes, maximal differentiation in the median and upper regions, and comparatively retarded development at the apex.

Within each spikelet, florets were distichously arranged along the rachilla and developed acropetally from the basal to the apical region. Each spikelet was subtended by a bract borne on the inflorescence axis. In lateral spikelets, the bract sequentially enclosed a hyaline, membranous prophyll, the glumes, and the florets. Along the rachilla, each glume and its associated floret occurred in an alternate, mutually enclosing arrangement. Terminal spikelets comprised 2–3 florets, with a mean of 2.8 ± 0.4, whereas the most fully developed lateral spikelets comprised 2–4 florets, with a mean of 3.0 ± 0.5 (Supplementary Fig. 2B). Each mature floret, from the exterior inward, consisted of one lemma, one palea, three lodicules, three stamens, and a single carpel. Transverse sections further illustrated the internal organization of spikelets and florets (Figure S3). The lemma was approximately 2.5–3.0 cm in length and exhibited

purple pigmentation across the dorsal region, extending toward the apex and margins. The palea was slightly shorter than the lemma and had two prominent keels, while the lodicules were hyaline, membranous, and approximately 3–4 mm long. Each stamen comprised a yellow anther supported by a white filament. The carpel consisted of a pale-yellow ovary, a white style, and a plumose and trifid stigma (Fig. 1F). During flowering, elongation of the filaments and style resulted in the exsertion of the anthers and stigmas beyond the glumes. Collectively, these morphological characteristics indicated that *P. reticulata* produced a compound inflorescence comprising spikelets, with spikelet and floret numbers varying among individuals and according to nodal position (Fig. 1; Supplementary Fig. 2).

Anatomical features of floral organogenesis

To elucidate the sequence of floret initiation and the developmental processes within spikelets of *P. reticulata*, serial histological sections were prepared from inflorescences and spikelets sampled at various stages of ontogenetic development (Fig. 2). Longitudinal sections revealed that spikelets located at different positions along the inflorescence axis exhibited distinct developmental states (Fig. 2A). Spikelet ontogeny could be broadly classified into four stages. During stage I, a spikelet primordium emerged on the inflorescence axis and was subtended by the outer bract. The primordium possessed a hemispherical apex with two conspicuous, regularly organized tunica cell layers (Fig. 2B). Due to the continued anticlinal divisions within the tunica, the spikelet primordium enlarged progressively, followed by the differentiation of glume and prophyll primordia, which gradually enclosed the apical meristem (Fig. 2C). During stage II, the terminal floret primordium was initiated first, followed by the sequential initiation of additional floret primordia in a basipetal direction. Within each developing floret, the lemma primordium differentiated first and subsequently enveloped with the floral meristem (Fig. 2D, E). During stage III, elongation of the spikelet rachilla internodes was accompanied by continued expansion of the floret primordia and progressive floral organogenesis. In addition, the basal florets exhibited a higher developmental rate, resulting in pronounced positional heterochrony among florets within the same spikelet (Fig. 2F, G). During stage IV, the florets underwent further elongation and approached maturity. Floral organ differentiation was most advanced in the basal florets and progressively less developed toward the spikelet apex. Moreover, a fourth floret primordium was occasionally detected in some spikelets (Fig. 2H, I). Thereafter, the meristematic activity of the spikelet apical meristem gradually declined, marking a developmental transition from floret primordium initiation to floral organ differentiation and maturation. Taken together, these anatomic observations demonstrated that the spikelet of *P. reticulata* can produce three to four florets. Floret primordia were initiated from the apex toward the base, whereas floral maturation proceeded more rapidly in basal than in apical florets, indicating a lack of concordance between the direction of primordium initiation and the gradient of floret maturation.

To further resolve the order of floral organ initiation in *P. reticulata* florets, we conducted serial histological sectioning of florets across various developmental stages (Fig. 2J - Q). During early floret initiation, the floral meristem exhibited a hemispherical configuration and was covered by a single, orderly arranged layer of tunica cells. Whereafter, active anticlinal and periclinal cell divisions sustained

meristematic proliferation, and the cells were characterized by their small size, dense cytoplasm, and intense staining (Fig. 2J). As the floral meristem continued to expand, floral organ primordia arose sequentially in a centripetal pattern. The lemma primordium was first to initiate on the abaxial periphery of the floral meristem and progressively enveloped the inner floral organs during elongation (Fig. 2J, K). Subsequently, the palea primordium emerged internal to the lemma and underwent continued elongation (Fig. 2L). Lodicule and stamen primordia were then initiated within the palea, the lodicules developed comparatively slowly and remained diminutive at maturity (Fig. 2M). The carpel primordium was the final organ primordium to arise, forming at the center of the floral meristem before progressively differentiating in coordination with stamen development (Fig. 2N, O). At later developmental stages, the elongating lemma and palea enclosed the lodicules, stamens, and carpel. As a result, the morphology and spatial organization of the floral organs became increasingly well defined (Fig. 2P). By the near-mature stage, the stamens and carpel elongated further, and the internal floral architecture was essentially established (Fig. 2Q). Collectively, these observations demonstrated that floral organogenesis in *P. reticulata* proceeded predominantly in a centripetal manner: lemma, palea, lodicules and stamens, followed by the carpel.

Male and female gametophyte development

To characterize male reproductive development, we systematically examined anther wall histogenesis, microsporogenesis, and male gametophyte development. The anthers contained four pollen sacs, and the anther wall consisted of four concentric layers: the epidermis, endothecium, middle layer, and tapetum. During early anther development, hypodermal cells underwent active mitotic divisions and differentiated into archesporial cells characterized by dense cytoplasm and conspicuous nuclei. These archesporial cells subsequently divided periclinally, generating outer primary parietal cells and inner primary sporogenous cells. The primary parietal cells differentiated further into the endothecium, middle layer, and tapetum, whereas the primary sporogenous cells proliferated and developed into microsporocytes, which were distinguished by their large size and dense protoplasmic contents (Fig. 3A - C). The microsporocytes underwent two consecutive meiotic divisions, producing dyads and tetrads. Within each tetrad, the four haploid microspores exhibited a planar tetragonal configuration before dissociating into free microspores (Fig. 3D - F). During subsequent development, the free microspores progressively enlarged, deposited thicker walls, and underwent nuclear migration toward the cell periphery, thereby entering the vacuolated uninucleate stage. Each microspore then experienced an asymmetric mitotic division to generate a vegetative cell and a generative cell, ultimately generating bicellular mature pollen grains (Fig. 3G - L). Microspore development was not completely synchronous, as well-developed pollen co-occurred with collapsed pollen within mature anthers. Such aberrant pollen was detected in all four pollen sacs (Supplementary Fig. 4).

The anther wall also exhibited distinct stage-dependent cytological changes. At the microsporocyte stage, the epidermis, endothecium, middle layer, and tapetum remained comparatively intact. Following the onset of meiosis, the endothecial and middle-layer cells became markedly compressed, accompanied by cytoplasmic depletion and reduced nuclear visibility, the middle layer became nearly

imperceptible, whereas the tapetum remained relatively well preserved. By the time of anther dehiscence, all anther wall layers except the epidermis were degenerated. Collectively, these observations uncovered that male reproductive development in *P. reticulata* progressed successfully to the bicellular pollen stage, although mature anthers contained a measurable proportion of morphologically aberrant pollen.

To elucidate the female reproductive development in *P. reticulata*, we conducted detailed observations of ovule ontogeny and megagametogenesis. The ovary was superior and unilocular, bearing a single hemitropous, bitegmic, and crassinucellate ovule. Following the differentiation of the carpel primordium, the carpel margins progressively fused to form the ovary, after which the ovule primordium arose from the placenta along the lateral ovarian wall. The nucellus differentiated first, followed sequentially by the initiation of the inner and outer integuments at its base. As development proceeded, both integuments gradually enveloped the nucellus, forming a micropyle, while the funiculus and raphe differentiated at the basal region of the ovule. During early ovule development, a conspicuous megaspore mother cell, characterized by a prominent nucleus and densely staining cytoplasm, differentiated within the nucellus (Fig. 3M - N). The megaspore mother cell subsequently underwent meiosis, producing a linearly arranged megaspore tetrad. One megaspore remained functional, whereas the other three were progressively degenerated (Fig. 3O). The functional megaspore then underwent three consecutive mitotic divisions, successively giving rise to two-nucleate, four-nucleate, and eight-nucleate embryo sacs. Following cellularization, the mature embryo sac comprised an egg apparatus, consisting of one egg cell and two synergids at the micropylar pole, three antipodal cells at the chalazal pole, and two polar nuclei within the central cell. Thus, the mature female gametophyte exhibited the typical polygonum-type organization, with eight nuclei arranged into seven cells (Fig. 3P - R). No discernible structural abnormalities were detected in the ovules or embryo sacs examined in this study. In contrast, collapsed and empty pollen grains were frequently observed within mature anthers, indicating that the reproductive defects identified in *P. reticulata* predominantly originated during male reproductive development.

Transcriptome sequencing, reference construction, and sample quality assessment

In the absence of a publicly available reference genome for *P. reticulata*, we therefore integrated PacBio single-molecule long-read sequencing with Illumina short-read sequencing to establish a non-redundant reference for transcriptome assay. The workflow for constructing the integrated reference transcriptome is summarized in Figure S5. PacBio sequencing generated 17,445,616 subreads, corresponding to 31.33 Gb of sequence data. CCS processing produced 271,264 consensus reads, of which 221,124 were classified as full-length non-chimeric (FLNC) reads, representing 81.52% of the CCS dataset. The N50 lengths of the CCS and FLNC reads were 2,246 bp and 2,173 bp, respectively. Following isoform clustering, sequence polishing, and Illumina-based error correction, the PacBio dataset provided high-quality, near-complete transcript models. Across the 18 Illumina libraries, a total of 400,091,502 clean read pairs (120.03 Gb) were retained, with individual libraries containing 19.41–24.81 million read pairs. The mean Q20 and Q30 scores were 98.02% and 94.40%, respectively, and the average GC content was

53.12%. Trinity-based *de novo* assembly of the Illumina reads generated 1,160,675 transcripts. Integration of these Illumina reads with the PacBio consensus sequences, followed by redundancy reduction at a 95% sequence-identity threshold, resulted in 971,143 merged transcript sequences. By further integrating homology search and Pfam domain evidence, TransDecoder predicted a total of 351,016 high-confidence protein-coding sequences. After an additional round of clustering at 95% sequence identity and source assignment, a final non-redundant set of 259,726 protein-coding sequences was obtained, comprising 34,106 PacBio-derived and 225,620 Trinity-derived sequences. BUSCO assessment against embryophyta_odb10 identified 91.1% complete, 6.1% fragmented, and 2.8% missing orthologs; assessment against poales_odb10 identified 92.6% complete, 3.0% fragmented, and 4.4% missing orthologs (Fig. 4A). Recovery of more than 90% complete BUSCOs in both assessments indicated broad coverage of conserved protein-coding genes in the sampled tissue. Simplified identifiers were assigned to the reference transcripts (Table S8).

To select samples suitable for subsequent expression analyses, we first performed PCA, hierarchical clustering, and Pearson correlation analysis on 28 Illumina libraries derived from seven tissue types (Table S1; Figure S6). The results showed that the four biological replicates of Lo were markedly dispersed in the overall expression space, with insufficient within-group correlation, and were therefore all excluded. In each of the remaining six tissue types, one library deviated from the within-group clustering: Nfl1, Fl3, Le2, Pa2, St3, and Ca4, respectively. After removing these samples, three biological replicates of each of Nfl, Fl, Le, Pa, St, and Ca were retained, yielding a total of 18 libraries, which were subsequently used for expression quantification, differential expression analysis, and weighted gene co-expression network analysis.

To evaluate intra-group reproducibility and inter-tissue transcriptional divergence among the 18 Illumina libraries retained for expression profiling, PCA and pairwise sample correlation analysis were conducted using the 5,000 transcripts exhibiting the highest expression variance. The first two principal components, PC1 and PC2, accounted for 34.11% and 27.86% of the total variance, respectively, explaining a cumulative 61.97% of the expression variability (Fig. 4B). The three biological replicates from each tissue generally clustered closely, the Nfl, Fl, Le, Pa, St, and Ca exhibited distinct tissue-specific segregation patterns. Consistently, the sample correlation heatmap demonstrated robust within-tissue clustering (Fig. 4C). Collectively, these findings confirmed the high intra-group concordance of the retained samples and demonstrated that their transcriptomic profiles effectively discriminate among the six tissue types.

After confirming the reproducibility among biological replicates, we performed 15 pairwise comparisons among the six tissue types using thresholds of padj < 0.01 and $|\log_2\text{FoldChange}| \geq 4$. In total, 33,765 unique differentially expressed transcripts (DETs) were identified, forming 1,970 exact intersection patterns; the 40 largest intersections are shown in Fig. 4D. The largest number of DETs was detected between Fl and St (14,488), followed by Fl versus Pa (12,062), Le versus Ca (11,713), Nfl versus St (11,645), Fl versus Le (10,882), and Pa versus Ca (10,738), indicating extensive transcriptional differences among tissues such as leaves, stamens, and carpels. In contrast, only 91 DETs were

detected between Le and Pa, substantially fewer than in the other tissue comparisons, suggesting that the lemma and palea had the most similar overall expression profiles. The UpSet analysis further showed that the largest exact intersection comprised 1,090 transcripts shared across all five comparisons between St and the other tissue types, reflecting a broad stamen-associated differential-expression pattern. Similarly, 891 and 577 transcripts were shared across all five comparisons involving Fl and Ca, respectively, revealing common differences between flowering leaves or carpels and the other tissues. In addition, 909, 874, 815, and 586 transcripts were exclusively detected in the Fl–St, St–Ca, Fl–Ca, and Nfl–St comparisons, respectively, demonstrating relatively distinct differential-expression patterns in specific tissue pairs. Overall, differential expression among the six tissue types comprised both shared tissue-associated patterns and patterns specific to particular tissue comparisons.

Screening and expression analysis of flowering regulatory genes

To assess whether transcriptional alterations in leaves at the flowering stage were associated with established hierarchical modules of flowering regulation, we used the flowering-regulatory architecture characterized in model plants as a reference. To this end, candidate homologous sequences from *P. reticulata* were mapped to multiple developmental processes including photoperiodic and circadian inputs, floral-signal integration, florigen transport, and shoot apical meristem responses. This analysis yielded a putative signaling network comprising 24 regulatory nodes (Fig. 5; Table S9). The inferred regulatory network linked the florigen-encoding genes *Hd3a* and *RFT1* to upstream integrators, including *Hd1*, *Ghd7*, and *Ehd1*, and further extended to floral meristem identity regulators, such as *OsFD* and *OsMADS14*/*15*.

Applying a threshold of $|\log_2 FC| \geq 1$ to the comparison between Nfl and Fl, candidates associated with 13 of the 24 nodes exhibited overall higher transcript abundance in Fl. These nodes included *SPA*, *COP1*, *Hd1*, *Ghd7*, *Ehd1*, *OsCO3*, *SPIN1-1*, *Hd3a*, *RFT1*, *OsFD*, *OsMADS55*, *OsMADS14*, and *OsMADS15*. By contrast, candidates corresponding to *OsMADS50* and *OsMADS56* were predominantly more highly expressed in Nfl, whereas candidates assigned to the remaining 9 nodes did not meet the specified differential-expression threshold. Thus, among the 15 nodes exhibiting threshold-level expression differences, 13 were upregulated in Fl, demonstrating that transcriptional divergence between Nfl and Fl spans multiple regulatory layers, including photoperiodic signal integration, florigen production and transport, and floral meristem responsiveness. Because *Ghd7* and *COP1* do not function uniformly as positive regulators of flowering, the elevated expression of their candidate homologs in Fl should be interpreted only as an association with the flowering-leaf state, rather than as direct evidence of a flowering-promotive role. The expression heatmap further revealed substantial gene-specific expression patterns among candidates assigned to the same regulatory node. For example, candidates homologous to *Hd3a* or *RFT1* accumulated predominantly in Fl, whereas several *OsMADS14*/*15*-associated candidates displayed higher expression in the lemma and palea. Candidates assigned to *OsID1*, *OsMADS51*, *LFL1*, and *RFL* also exhibited distinct organ-preferential expression profiles. To sum up, these findings indicated that transcriptional differences between flowering and non-flowering leaves of *P.*

reticulata encompassed multiple successive layers of the canonical flowering-regulatory framework and were accompanied by pronounced tissue-specific expression divergence among homologous gene family members.

Candidate transcripts associated with floral organ identity and morphogenesis

To identify putative genes involved in floral organ identity specification, we conducted phylogenetic analyses of MADS-box proteins from rice, moso bamboo, and *P. reticulata*. This analysis identified 38 candidate sequences representing the ABCDE(G) functional classes (Fig. 6A; Figure S7). Specifically, classes A (AP1/FUL-like), B (AP3/PI-like), C (AG-like), D (AGL11/STK-like), E (SEP-like), and G (AGL6-like) comprised 9, 9, 5, 3, 9, and 3 candidates, respectively. Phylogenetic reconstruction placed the class A candidates within the grass-specific FUL-like clade, whereas the class C and D candidates grouped with the OsMADS3/58 and OsMADS13/21 reference sequences, respectively, thereby resolving the C- and D-class lineages as phylogenetically distinct groups. Collectively, these candidates covered the major MADS-box lineages associated with the ABCDE(G) model of floral organ identity determination.

Our expression profiling revealed substantial transcriptional divergence among members of the same MADS-box subclass (Fig. 6B, C; Table S10). Within class A, *Pre143263807* and *Pre108790797* exhibited broad expression patterns. *Pre143263807* was expressed preferentially in Pa, Fl, and Ca, whereas *Pre108790797* reached its highest transcript abundance in Ca. *Pre97976702*, *Pre52669c0g2i3*, *Pre78907020*, and *Pre128714702* were predominantly expressed in Pa and Le, with variable transcriptional levels in Fl. By contrast, *Pre184736c0g2i2*, *Pre13924c0g1i5*, and *Pre159582648* displayed generally low expression levels, although *Pre184736c0g2i2* and *Pre13924c0g1i5* preferentially expressed in Pa or Le. Class B candidates showed heterogeneous expression profiles across Le, Pa, and St. Pre15993612 and Pre20993c0g1i4 had their highest mean expression in Le, followed by St. Pre31400c0g2i7 showed the same ordering, with mean TPM values of 104.87 in Le, 47.55 in St, and 29.49 in Pa. Pre20993c0g1i2 was more highly expressed in Le and Pa, whereas Pre66650761 had its highest mean expression in Le (22.14 TPM), followed by similar levels in Pa and St (15.47 and 15.39 TPM, respectively). Pre2938c0g1i2 had its highest mean expression in Ca and Le. Pre27593190 showed relatively low transcript abundance overall but reached its highest mean levels in Pa and Le (5.44 and 4.85 TPM, respectively). Pre2938c0g1i10 was preferentially expressed in Fl and Ca. Pre2938c0g1i12 was also a low-abundance transcript, with its highest mean TPM in Le (1.20), followed by Ca (0.91) and Pa (0.87). The five class C (AG-like) transcripts all reached their highest mean TPM in Ca, although the degree of carpel preference varied among members. Pre14353407 and Pre37522c0g1i4 showed pronounced Ca-preferential expression. Pre46991101 was also expressed in Pa and Le, whereas Pre138084544 had almost identical mean TPM values in Ca and Le (89.43 and 88.98, respectively) and was additionally expressed in Pa and St. Pre37522c0g2i1 showed a broader expression pattern encompassing Ca, Le, and St. The class D genes *Pre38471c1g1i2*, *Pre35719c0g2i3*, and *Pre35719c0g1i1* were also strongly enriched in Ca. Within class E, *Pre159581399*, *Pre30617c0g1i1*, *Pre30617c0g1i8*, and *Pre144509572* were predominantly expressed in Ca; *Pre29000c0g1i3* exhibited a broader expression

domain in Pa, Le, and Ca, and *Pre31c2g1i7*, *Pre49539c0g3i4*, *Pre179570236*, and *Pre2884356* were preferentially expressed in Pa and Le. The class G genes *Pre41448c0g1i1*, *Pre41448c0g1i5*, and *Pre13173739* showed maximal transcript abundance in Pa, followed by Ca and Le, with comparatively low expression in leaves and St. Collectively, although the subclasses showed organ-associated expression tendencies, individual members differed in both abundance and tissue preference. Following Benjamini–Hochberg (BH) correction, the Friedman test identified significant overall differences among tissues at the subclass level for classes A, B, C, D, E, and G, with adjusted *P* values of 1.03×10^{-4}, 1.03×10^{-3}, 6.92×10^{-4}, 0.0140, 1.03×10^{-4}, and 0.0141, respectively (Fig. 6C). Integrative analysis of phylogenetic relationships and tissue-specific expression profiles revealed distinct class-dependent patterns. Class A candidates showed varied expression in flowering leaves and floral organs, while class B candidates were preferentially expressed in lemmas, paleas, and, for several members, stamens, classes C and D were prominently enriched in carpels, although their constituent members differed in expression levels, class E candidates displayed broad expression across multiple floral whorls, and class G candidates showed a pronounced expression pattern toward the palea. These findings demonstrated that the ABCDE(G)-class candidate genes in *P. reticulata* exhibit substantial expression divergence at both the subclass and individual-member levels across the six examined tissues, thereby establishing an expression-based association between floral organ morphology and putative organ-identity genes.

To delineate organ-associated co-expression networks, we performed WGCNA analysis, which classified the transcripts into 17 co-expression modules (ME1 - ME17) (Fig. 7A). Our analysis revealed that ME14 exhibited the strongest association with Ca ($r = 0.98$, $P = 2 \times 10^{-13}$) and was also positively associated with the composite reproductive trait of Ca_St ($r = 0.62$, $P = 0.007$). ME1 was significantly and positively correlated with St ($r = 0.79$, $P = 9 \times 10^{-5}$), whereas ME12 showed a strong positive correlation with Le_Pa ($r = 0.97$, $P = 9 \times 10^{-11}$). ME5 was positively associated with leaves ($r = 0.86$, $P = 6 \times 10^{-6}$) but negatively associated with the composite floral-organ trait ($r = -0.86$, $P = 6 \times 10^{-6}$). In contrast, ME17 was positively correlated with both Ca_St ($r = 0.81$, $P = 5 \times 10^{-5}$) and the composite floral-organ trait ($r = 0.72$, $P = 7 \times 10^{-4}$). Our findings hence demonstrated that carpels, stamens, lemmas and paleas, and leaves are characterized by distinct co-expression modules, while male and female reproductive organs shared common transcriptional programs.

To elucidate the associated genes involved in organ development-related modules, we further examined representative annotation categories and highly connected candidate genes within ME14 and ME1 (Table S2). The Ca linked module ME14 was enriched in annotations corresponding to OVATE family transcriptional repressors, fasciclin domain-containing proteins, hydroxyproline-rich glycoproteins, gibberellin-regulated proteins, senescence-associated regulators, and pectin methylesterase inhibitors (Table S5). These functional genes were implicated in organ morphogenesis, cell-wall remodeling, and phytohormone responses. The *GASA4-like*, *OFP14-like*, *OFP8-like*, *D4655c*, and *K18L3.4* exhibited high connectivity within the candidate network (Fig. 7B, C). By contrast, the stamen-associated module ME1 contained annotations for Ole e I-like pollen proteins, MADS-box transcription factors, PISTILLATA-like, LBD transcription factors, the PIN9 auxin transporter, ethylene-responsive factors, and B3 domain-containing DNA-binding proteins (Table S7). *AGL104_1*, *AGL104_2*, *AGL66*, *Ole_e_1*, *Lol_p_11*, and *YUC2*

were highly enriched and expressed in this module (Fig. 7B, D). Collectively, ME14 predominantly captured transcripts associated with carpel or ovary growth, cell-wall dynamics, and hormone responses, whereas ME1 integrated candidates involved in floral organ identity specification, pollen development, and hormonal regulation. ME12, ME17, and ME5 respectively complement the expression programs of lemmas and paleas, male and female reproductive organs, and leaves (Tables S3, S4, S6). As a result, these findings resolved essential and distinct co-expression regulatory modules in elucidation of the organ development and differentiation of *P. reticulata*.

Discussion

Developmental characteristics of Phyllostachys reticulata inflorescences

The *P. reticulata* inflorescence exhibited distinct spatial patterns of primordium initiation, subsequent growth, and maturation. Floret primordia were initiated from the apex toward the base, whereas basal florets matured earlier than apical florets. Together with the positional arrest of spikelet development along the inflorescence axis, this difference between initiation and maturation highlights the need to distinguish developmental stage from mature architecture when interpreting bamboo inflorescences [22, 23]. It also accounted for the simultaneous occurrence of actively developing spikelets, developmentally arrested spikelets, and latent buds within a single inflorescence, as well as positional variation in the developmental progression of florets within an individual spikelet. It has been recorded that an inflorescence of *P. reticulata* usually contained 5–7 spikelets [38]. Our study revealed that an inflorescence usually contains 4–8 units, of which 3–5 spikelets continued to develop, while 1–3 basal units remained in the latent-bud state. The difference between these two statistical approaches indicated that investigations carried out at maturity stage may obscure the actual developmental situation along the inflorescence axis if arrested units are not clearly distinguished.

Terminal spikelets were diagnostically characterized by the absence of a prophyll, whereas prophylls were consistently present in lateral spikelets. The hierarchical arrangement of bracts, spikelets, and florets formed the architectural framework of the compound inflorescences typical of woody bamboos, with their complex structure arising from the iterative deployment of modular branching units [22, 23, 64]. Floret number per spikelet in *P. reticulata* exhibited a degree of variability rather than strict constancy. Terminal spikelets contained two to three florets, whereas fully developed lateral spikelets contained two to four florets. Nevertheless, the mean floret number in both spikelet types was approximately three. Each floret possessed three stamens. Although stamen number and pistil morphology in *P. reticulata* were generally consistent with the floral characteristics typical of other *Phyllostachys* species, marked interspecific variation was observed in floret number and other floral-organ traits, highlighting the substantial structural diversity of bamboo spikelets and flowers [6, 34, 65, 66]. In Poaceae, inflorescence architecture was determined by the relative chronology of meristem identity transitions and the progressive establishment of determinacy across sequential branching orders [67]. Accordingly, the node-specific developmental heterogeneity observed in *P. reticulata* was more plausibly ascribed to heterochronic differences in the acquisition of meristem determinacy at

successive hierarchical levels than to mere variation in the dimensions of mature organs. The “inflorescence-spikelet-floret” model thus defined the nested architectural framework within which floral morphogenesis unfolds in *P. reticulata* (Fig. 8).

Gametophyte development and its implications for low seed set

Following floral-organ initiation, microsporogenesis and male gametophyte development in *P. reticulata* proceeded through archesporial and microspore mother cells, dyads, tetrads and free microspores, culminating in bicellular mature pollen. Female reproductive development encompassed the megaspore mother cell, linear megaspore tetrad and functional megaspore stages, followed by two-, four- and eight-nucleate embryo sacs and the formation of a seven-celled, eight-nucleate Polygonum-type embryo sac, as described in our histological results. The sequence of microspore formation broadly resembles that described in *P. praecox* [68], *Bambusa tuldoides* [65] and *Pleioblastus pygmaeus* [69], although these species were reported to produce tricellular mature pollen. Both bicellular and tricellular mature pollen have been reported in *Pseudosasa viridula* [70] and *P. nigra* [71], whereas *B. textilis* was reported to contain mature pollen with two or three nuclei [34]. On the female side, Polygonum-type embryo-sac development has been documented in *P. viridula* [70]; *P. pygmaeus* also passes through a seven-celled, eight-nucleate stage, followed by antipodal proliferation [69]. Thus, similarities in the developmental sequence do not imply identical mature gametophyte organization across bamboo species. The open florets, exserted anthers and trilobed plumose stigmas of *P. reticulata* represent morphological adaptations consistent with anemophilous pollination. Nevertheless, the occurrence of shriveled and empty pollen grains within mature anthers indicates that morphological progression to maturity does not necessarily ensure the functional viability of all pollen grains. Comparable pollen-development abnormalities have been reported in *B. oldhamii* ‘Xia Zao’ and *P. nigra* [71, 72], and pollen performance in *P. nigra* also varies with sampling stage and germination conditions [73].

Low seed set cannot be attributed to a single, discrete stage within the reproductive developmental program; rather, it is governed by the combined effects of multiple factors, including pollen availability, pollen dehiscence and dispersal, pollen deposition on receptive stigmas, cross-pollination efficiency, and favorable environmental conditions. Long-term investigations of *P. reticulata* demonstrated that *in vitro* pollen germination rates were generally below 30%, which was associated with reduced stigmatic pollen loads and low natural seed-set rates [38]. Consistent with these findings, studies of other *Phyllostachys* species and woody bamboos have reported the co-occurrence of diminished pollen viability, abnormal anther or microgametophyte development, and inadequate seed production [71, 72, 74]. Moreover, sporadic or asynchronous flowering decreases the density of concurrently flowering genotypes, thereby constraining the availability of outcross pollen. Even during mass-flowering events in bamboos, clonal structure and pollen-mediated gene flow can influence self-pollination rates and subsequent seed formation [75, 76]. In this study, phenological variation in maturation among spikelets at distinct nodal positions and among florets within spikelets revealed pronounced intra-plant temporal heterogeneity in

pollen dehiscence and stigma receptivity. Together, these observations suggest that aberrant pollen morphology and temporal heterogeneity in reproductive development may contribute to low seed set. Direct measurements of pollen viability, germination, pollination success, and seed formation are needed to establish their relative contributions in the sampled plants.

Comparison of flowering regulatory frameworks in Phyllostachys reticulata and model plants

The increasing availability of full-length transcriptomic and genomic datasets for bamboo species has substantially enhanced the feasibility of cross-species homolog assignment [2, 77]. Given the absence of a reference genome for *P. reticulata*, we integrated PacBio long-read and Illumina short-read sequencing technologies to generate a non-redundant reference set of protein-coding transcripts, thereby providing a robust genetic resource for identifying and characterizing differentially expressed genes associated with reproductive development in *P. reticulata*.

Transcriptomic profiles of Nfl and Fl were clearly differentiated, indicating extensive transcriptional changes associated with the flowering-branch state. As illustrated in Fig. 5, P. *reticulata* transcripts homologous to the rice flowering regulators Hd1, Ghd7, Ehd1, Hd3a/RFT1, OsFD, and OsMADS14/15 generally accumulated at higher levels in Fl. These expression patterns were consistent with coordinated transcriptional changes involving photoperiodic signal integration, florigen production and transport, and floral meristem identity, although they did not establish direct regulatory relationships. Comparable involvement of photoperiodic, FT/PEBP, SOC1/SVP, and MADS-box pathways in bamboo reproductive transition has been reported in transcriptomic studies of several bamboo species [11–13]. Proteomic studies and functional analyses of individual flowering regulators provide further support for the involvement of these conserved pathways in bamboos [17, 20, 78]. *Hd1* exerts photoperiod-dependent dual functions in flowering regulation, acting either as an activator or a repressor according to day length and genetic background. It modulates *Ehd1* transcription through interactions with *Ghd7* and *DTH8* [55, 57, 79]. *OsLHY* and cytokinin-associated regulation further connect circadian and hormonal signals with flowering pathways in rice [80, 81]. Florigen proteins produced in leaves move to the shoot apex, where Hd3a interacts with 14-3-3 proteins and OsFD1 to form a florigen activation complex that activates downstream floral meristem identity genes [59]. Subsequently, FT-L1-like proteins further consolidate the transition to reproductive development and promote inflorescence meristem determinacy [59, 82, 83]. Expression studies in rice have shown that *FUL-like* genes respond to florigen earlier than SEP/AGL-class floral organ identity genes [84]. In our study, *FUL-like* candidate genes were predominantly associated with differences in flowering status between Nfl and Fl, whereas SEP/AGL-class candidates exhibited stronger floral organ-specific expression patterns. These findings suggested that the two gene groups may function preferentially in floral transition and subsequent floral organogenesis, respectively, in *P. reticulata*. Furthermore, the *P. reticulata* homologs of *OsMADS50* and *OsMADS56* were highly expressed in Nfl, indicating that *SOC1-like* genes may coordinate the balance between floral transition and organ assembly through distinct combinatorial interactions among family members.

Organ-specific expression of ABCDE(G)-class MADS-box genes

Our WGCNA analysis further delineated organ-specific co-expression modules. The carpel-associated ME14 module was enriched in *GASA4-like*, *OFP14-like*, and *OFP8-like* genes, together with multiple candidates implicated in cell-wall dynamics. These genes are associated with cell expansion, cell adhesion, cell-wall remodeling, and organ morphogenesis, consistent with the developmental characteristics of the ovary and carpel. In contrast, the stamen-associated ME1 module comprised candidate genes encoding PISTILLATA-like MADS-box transcription factors, *AGL66*, *AGL104*, Ole e I-like pollen proteins, and *YUC2*. In *Arabidopsis thaliana*, the MIKC-type MADS-box genes, *AGL66* and *AGL104* contribute to transcriptional regulation and the germination of mature pollen [85, 86]. Their co-clustering within ME1 supports an association of this module with pollen development. Because the expression analysis compared tissues rather than normal and abnormal anthers, it does not establish a relationship between these candidates and aberrant pollen formation. Their specific functions in *P. reticulata* require further validation. ME12 exhibited a strong correlation with the lemma-palea group (Le_Pa), while only a limited number of differentially expressed genes were identified between the lemma and palea. These findings suggested that the two floral organs share a broadly similar transcriptional landscape while retaining a subset of tissue-specific expression features.

Phylogenetic analysis placed the candidate MADS-box transcripts within the grass ABCDE(G) floral-development framework. All A-class genes identified in *P. reticulata* clustered within the AP1/FUL-like lineage. Several members were more highly expressed in Fl than in Nfl, whereas individual transcripts showed distinct preferences for Le, Pa, or Ca. This expression profile was consistent with the established functions of rice *OsMADS14/15/18/20* in integrating florigen signaling with meristem phase transition and outer-whorl organ specification [29, 87, 88]. B-class candidates, including *SPW1/OsMADS16/2/4*-like homologs, showed heterogeneous expression across Le, Pa, and St [89]. C-class candidates reached their highest mean expression in Ca, although some members also showed substantial expression in Le, Pa, or St, in agreement with the roles of *OsMADS3/58* in specifying carpel and stamen identity and regulating floral meristem determinacy. D-class genes were nearly undetectable in leaves but were strongly enriched in Ca, consistent with the established role of OsMADS13 in ovule identity specification [90]. E-class genes were broadly and abundantly expressed in Ca, Pa, and Le, supporting the function of rice SEP-like proteins in the development of multiple floral whorls [91]. G-class genes were most prominently expressed in Pa, with their expression pattern extending to Ca and Le, consistent with the involvement of *OsMADS6* in the specification of palea, lodicule, ovule, and floral meristem identity [27].

Bamboo ABCDE-class homologues largely preserve the rice-like phylogenetic architecture, although lineage-specific variation has emerged in gene number and organ-specific expression pattern [30–32, 92, 93]. The putative MADS-box genes identified in *P. reticulata* were assigned to the evolutionarily conserved A-, B-, C-, D-, E-, and G-class lineages of angiosperms. Nevertheless, individual classes and their

constituent members exhibited distinct transcript abundance and spatial expression profiles across the palea, lemma, stamens, and pistil. These findings suggest that, despite their conserved phylogenetic affiliations, these genes have undergone regulatory divergence in expression level and pattern during floral organogenesis [28, 94, 95]. The 38 candidate transcripts identified in *P. reticulata* were profiled across six tissues. A-class genes established a transcriptional link between the flowering-leaf state and outer-whorl organ development; B- and C-class candidates showed expression patterns consistent with potential roles in stamen-associated programs; C- and D-class genes were implicated in carpel and ovule development; E-class genes were broadly enriched in organogenetic processes; and G-class genes were preferentially associated with palea-related developmental programs. Because the transcriptome reference used in this study was assembled *de novo* without a corresponding reference genome, the number of identified candidates could be overestimated owing to the inclusion of alternative splice isoforms, allelic variants, or highly similar paralogous transcripts. Future integration of a chromosome-scale genome assembly with in situ expression assays will facilitate the resolution of gene-copy relationships and cell-type-specific expression patterns [2]. Collectively, the transcriptome assay delineated a developmental framework extending from the directional differentiation of inflorescences and florets, through the photoperiod-florigen-like transcriptional state of flowering leaves and organ-specific co-expression modules, to the functional partitioning of floral organ identity among ABCDE(G)-class MADS-box genes.

Conclusions

This study establishes an integrated morphological and transcriptional framework for floral development in *Phyllostachys reticulata*. Serial morphological and histological observations distinguished the directions of floret primordium initiation and subsequent maturation, documented centripetal floral organogenesis, and characterized gametophyte development and pollen abnormalities, providing an anatomical basis for investigating reproduction in this species. Integration of PacBio long-read and Illumina short-read sequencing generated a reference transcriptome comprising 259,726 non-redundant protein-coding sequences, providing a sequence resource for bamboo reproductive research. Tissue-level expression analyses further distinguished flowering-state-associated expression patterns from those associated with floral organs, identified 38 candidate ABCDE(G)-class MADS-box transcripts, and delineated organ-associated co-expression modules. These findings connect developmental observations with candidate transcriptional programs and provide a basis for comparing conservation and divergence in bamboo floral development. Future research could prioritize functional characterization of candidate MADS-box genes in stamen and carpel development and combine pollen viability assays, in vitro germination tests, and controlled pollination experiments to determine whether impaired pollen function is a major factor limiting seed set in *P. reticulata*.

Abbreviations

BUSCO
Benchmarking Universal Single-Copy Orthologs

Ca
carpels
CCS
circular consensus sequencing
DETs
differentially expressed transcripts
FAA
formalin–acetic acid–alcohol
Fl
leaves from flowering branches
FLNC
full-length non-chimeric
GS
gene significance
GSA
Genome Sequence Archive
Le
lemmas
Lo
lodicules
MAD
median absolute deviation
MM
module membership
Nfl
leaves from non-flowering branches
ORFs
open reading frames
Pa
paleae
padj
adjusted P value
PCA
principal component analysis
SD
standard deviation
St
stamens
TPM
transcripts per million

WGCNA
weighted gene co-expression network analysis.

Declarations

Ethics approval and consent to participate

Not applicable.

Consent for publication

Not applicable.

Competing interests

The authors declare that they have no competing interests.

Funding

This work was supported by the National Natural Science Foundation of China (39160051, 32260058) and the Natural Science Foundation of Jiangxi Province (20192ACB21005, 20232BAB215008).

Author Contribution

Yonglong Li and Xujie Huang contributed equally to this work. Yonglong Li performed data analysis and wrote the original manuscript. Xujie Huang performed data analysis. Heng Liu contributed to early-stage sample collection and histological sectioning. Chengkun Wang and Jiajing Peng contributed to portions of the data analysis. Wengen Zhang contributed to the acquisition of plant material. Chunce Guo guided the data analysis and the development of the manuscript structure. Meixia Wang guided the development of the manuscript structure and scientific writing. All authors read and approved the final manuscript.

Acknowledgement

We sincerely thank Lihan Hou, Lili Shen, and Fengjiao Li for their valuable assistance and patient support during sample collection and processing. Their time and effort contributed greatly to the completion of this work. We are especially grateful to Professor Fen Yu for her patient and thoughtful guidance on histological sectioning and microscopic observations, which greatly assisted us in preparing and

examining the specimens. We also extend our sincere appreciation to Professor Guangyao Yang for lending his taxonomic expertise to the identification of the bamboo species studied. We deeply appreciate the time, care, and expertise that they generously shared throughout this research.

Data Availability

The raw sequencing data generated in this study have been deposited in the Genome Sequence Archive (GSA) at the National Genomics Data Center under accession number CRA051791 (https://ngdc.cncb.ac.cn/gsa/browse/CRA051791), associated with BioProject PRJCA076804. The data are currently under embargo and are scheduled for public release on June 1, 2027.

References

1. Wu C, Cheng Z, Gao J. Mysterious bamboo flowering phenomenon: a literature review and new perspectives. Sci Total Environ. 2024;911:168695. https://doi.org/10.1016/j.scitotenv.2023.168695.
2. Wang W, Wu Q, Wang N, Ye S, Wang Y, Zhang J, et al. Advances in bamboo genomics: growth and development, stress tolerance, and genetic engineering. J Integr Plant Biol. 2025;67:1725–55. https://doi.org/10.1111/jipb.13909.
3. Tucker MR, Koltunow AMG. Sexual and asexual (apomictic) seed development in flowering plants: molecular, morphological and evolutionary relationships. Funct Plant Biol. 2009;36:490–504. https://doi.org/10.1071/FP09078.
4. Janzen DH. Why bamboos wait so long to flower. Annu Rev Ecol Syst. 1976;7:347–91. https://doi.org/10.1146/annurev.es.07.110176.002023.
5. Zheng X, Lin S, Fu H, Wan Y, Ding Y. The bamboo flowering cycle sheds light on flowering diversity. Front Plant Sci. 2020;11:381. https://doi.org/10.3389/fpls.2020.00381.
6. Wang X, Liu J, Zhao C, Wang S. Morphological characteristics of floral organs and their taxonomic significance in 23 species of bamboo from Southwest China. Plants (Basel). 2025;14:3751. https://doi.org/10.3390/plants14243751.
7. Keeley JE, Bond WJ. Mast flowering and semelparity in bamboos: the bamboo fire cycle hypothesis. Am Nat. 1999;154:383–91. https://doi.org/10.1086/303243.
8. Fornara F, de Montaigu A, Coupland G. SnapShot: control of flowering in Arabidopsis. Cell. 2010;141:550–550. https://doi.org/10.1016/j.cell.2010.04.024. .e2.
9. Higgins JA, Bailey PC, Laurie DA. Comparative genomics of flowering time pathways using Brachypodium distachyon as a model for the temperate grasses. PLoS ONE. 2010;5:e10065. https://doi.org/10.1371/journal.pone.0010065.
10. Tsuji H, Taoka KI, Shimamoto K. Regulation of flowering in rice: two florigen genes, a complex gene network, and natural variation. Curr Opin Plant Biol. 2011;14:45–52. https://doi.org/10.1016/j.pbi.2010.08.016.

11. Ge W, Zhang Y, Cheng Z, Hou D, Li X, Gao J. Main regulatory pathways, key genes and microRNAs involved in flower formation and development of moso bamboo (Phyllostachys edulis). Plant Biotechnol J. 2017;15:82–96. https://doi.org/10.1111/pbi.12593.
12. Wang X, Wang Y, Yang G, Zhao L, Zhang X, Li D, et al. Complementary transcriptome and proteome analyses provide insight into the floral transition in bamboo (Dendrocalamus latiflorus Munro). Int J Mol Sci. 2020;21:8430. https://doi.org/10.3390/ijms21228430.
13. Zhao W, Guo C, Yao W, Zhang L, Ding Y, Yang Z, et al. Comparative phylogenomic analyses and co-expression gene network reveal insights in flowering time and aborted meiosis in woody bamboo, Bambusa oldhamii 'Xia Zao' ZSX. Front Plant Sci. 2022;13:1023240. https://doi.org/10.3389/fpls.2022.1023240.
14. Guo XQ, Wang Y, Wang Q, Xu ZE, Lin XC. Molecular characterization of FLOWERING LOCUS T (FT) genes from bamboo (Phyllostachys violascens). J Plant Biochem Biotechnol. 2016;25:168–78. https://doi.org/10.1007/s13562-015-0322-x.
15. Dutta S, Biswas P, Chakraborty S, Mitra D, Pal A, Das M. Identification, characterization and gene expression analyses of important flowering genes related to photoperiodic pathway in bamboo. BMC Genomics. 2018;19:190. https://doi.org/10.1186/s12864-018-4571-7.
16. Xiao G, Li B, Chen H, Chen W, Wang Z, Mao B, et al. Overexpression of PvCO1, a bamboo CONSTANS-LIKE gene, delays flowering by reducing expression of the FT gene in transgenic Arabidopsis. BMC Plant Biol. 2018;18:232. https://doi.org/10.1186/s12870-018-1469-0.
17. Hou D, Li L, Ma T, Pei J, Zhao Z, Lu M, et al. The SOC1-like gene BoMADS50 is associated with the flowering of Bambusa oldhamii. Hortic Res. 2021;8:133. https://doi.org/10.1038/s41438-021-00557-4.
18. Cheng Z, Hou D, Liu J, Li X, Xie L, Ma Y, et al. Characterization of moso bamboo (Phyllostachys edulis) Dof transcription factors in floral development and abiotic stress responses. Genome. 2018;61:151–6. https://doi.org/10.1139/gen-2017-0189.
19. Liu J, Cheng Z, Xie L, Li X, Gao J. Multifaceted role of PheDof12-1 in the regulation of flowering time and abiotic stress responses in moso bamboo (Phyllostachys edulis). Int J Mol Sci. 2019;20:424. https://doi.org/10.3390/ijms20020424.
20. Liu S, Vasupalli N, Hou D, Lin X. Ectopic expression of a bamboo SVP-like gene alters flowering time and floral organs in Arabidopsis thaliana. Plant Cell Tissue Organ Cult. 2022;150:721–32. https://doi.org/10.1007/s11240-022-02343-z.
21. Liu S, Hou D, Vasupalli N, Lin X. Overexpression of PvSVP1, an SVP-like gene of bamboo, causes early flowering and abnormal floral organs in Arabidopsis and rice. Acta Biochim Biophys Sin (Shanghai). 2023;55:237–49. https://doi.org/10.3724/abbs.2022199.
22. Lin SY, Wan YW, Fu HJ, Zhang L, Jiang MY, Yin ZF, et al. Research on inflorescence establishment and revision of inflorescence type in bamboo plants. J Nanjing Univ Nat Sci Ed. 2018;42:1–6. https://doi.org/10.3969/j.issn.1000-2006.201801053.

23. Cai ZY, Xia NH. A novel elucidation for synflorescences of Chinese bamboos. Plants (Basel). 2024;13:29. https://doi.org/10.3390/plants13010029.
24. Shan H, Cheng J, Zhang R, Yao X, Kong H. Developmental mechanisms involved in the diversification of flowers. Nat Plants. 2019;5:917–23. https://doi.org/10.1038/s41477-019-0498-5.
25. Coen ES, Meyerowitz EM. The war of the whorls: genetic interactions controlling flower development. Nature. 1991;353:31–7. https://doi.org/10.1038/353031a0.
26. Theißen G, Saedler H. Floral quartets. Nature. 2001;409:469–71. https://doi.org/10.1038/35054172.
27. Li H, Liang W, Jia R, Yin C, Zong J, Kong H, et al. The AGL6-like gene OsMADS6 regulates floral organ and meristem identities in rice. Cell Res. 2010;20:299–313. https://doi.org/10.1038/cr.2009.143.
28. Smaczniak C, Immink RGH, Angenent GC, Kaufmann K. Developmental and evolutionary diversity of plant MADS-domain factors: insights from recent studies. Development. 2012;139:3081–98. https://doi.org/10.1242/dev.074674.
29. Lin EP, Peng HZ, Jin QY, Deng MJ, Li T, Xiao XC, et al. Identification and characterization of two bamboo (Phyllostachys praecox) AP1/SQUA-like MADS-box genes during floral transition. Planta. 2009;231:109–20. https://doi.org/10.1007/s00425-009-1033-0.
30. Shih MC, Chou ML, Yue JJ, Hsu CT, Chang WJ, Ko SS, et al. BeMADS1 is a key to delivery MADSs into nucleus in reproductive tissues: de novo characterization of Bambusa edulis transcriptome and study of MADS genes in bamboo floral development. BMC Plant Biol. 2014;14:179. https://doi.org/10.1186/1471-2229-14-179.
31. Cheng Z, Ge W, Li L, Hou D, Ma Y, Liu J, et al. Analysis of MADS-box gene family reveals conservation in floral organ ABCDE model of moso bamboo (Phyllostachys edulis). Front Plant Sci. 2017;8:656. https://doi.org/10.3389/fpls.2017.00656.
32. Yang D, Yang J, Wan J, Xu Y, Li L, Rong J, et al. Genome-wide identification of MIKCc-type MADS-box family gene and floral organ transcriptome characterization in Ma bamboo (Dendrocalamus latiflorus Munro). Genes (Basel). 2023;14:78. https://doi.org/10.3390/genes14010078.
33. Huang L, Deng L, Chu C, Zhan H, Wang S. Morphological and anatomical observations of floral organs and sterility analysis of Fargesia yuanjiangensis. Sci Silvae Sin. 2020;56:64–73. https://doi.org/10.11707/j.1001-7488.20200407.
34. Yan YD, Zhou L, Wang SG. Floral morphology and development of female and male gametophytes of Bambusa textilis. Res. 2024;37:150–8. https://doi.org/10.12403/j.1001-1498.20230222.
35. Wang ZP, Stapleton CMA. Phyllostachys. In: Wu ZY, Raven PH, Hong DY, editors. Flora of China. Volume 22: Poaceae. Beijing: Science; St. Louis: Missouri Botanical Garden Press;; 2006. pp. 163–80.
36. Zhang XM, Sheng WP. A study of improved bamboo species in Yiyang City, Hunan Province. World Bamboo Rattan. 2011;9:23–6. https://doi.org/10.13640/j.cnki.wbr.2011.02.016.
37. Chan KN, Liang Z, Kisvarga S, Veres A, Hamar-Farkas D, Orlóci L, et al. Shoot phenology in Bambusoideae: a review. Int J Plant Biol. 2022;13:579–97. https://doi.org/10.3390/ijpb13040046.

38. Zhang WY, Ma NX, Wu LL, Huang ST, Zhang JW. A study of flowering and fruiting of Phyllostachys bambusoides. J Bamboo Res. 1992;11:15–25.
39. Sun LF, Guo QR, Wang Q, Feng Y, Mu SH. Flower organs morphology and structure of Phyllostachys edulis. Sci Silvae Sin. 2012;48:124–9. https://doi.org/10.11707/j.1001-7488.20121120.
40. Eid J, Fehr A, Gray J, Luong K, Lyle J, Otto G, et al. Real-time DNA sequencing from single polymerase molecules. Science. 2009;323:133–8. https://doi.org/10.1126/science.1162986.
41. Chen S, Zhou Y, Chen Y, Gu J. fastp: an ultra-fast all-in-one FASTQ preprocessor. Bioinformatics. 2018;34:i884–90. https://doi.org/10.1093/bioinformatics/bty560.
42. Salmela L, Rivals E. LoRDEC: accurate and efficient long read error correction. Bioinformatics. 2014;30:3506–14. https://doi.org/10.1093/bioinformatics/btu538.
43. Grabherr MG, Haas BJ, Yassour M, Levin JZ, Thompson DA, Amit I, et al. Full-length transcriptome assembly from RNA-seq data without a reference genome. Nat Biotechnol. 2011;29:644–52. https://doi.org/10.1038/nbt.1883.
44. Haas BJ, Papanicolaou A, Yassour M, Grabherr M, Blood PD, Bowden J, et al. De novo transcript sequence reconstruction from RNA-seq using the Trinity platform for reference generation and analysis. Nat Protoc. 2013;8:1494–512. https://doi.org/10.1038/nprot.2013.084.
45. Fu L, Niu B, Zhu Z, Wu S, Li W. CD-HIT: accelerated for clustering the next-generation sequencing data. Bioinformatics. 2012;28:3150–2. https://doi.org/10.1093/bioinformatics/bts565.
46. Buchfink B, Reuter K, Drost HG. Sensitive protein alignments at tree-of-life scale using DIAMOND. Nat Methods. 2021;18:366–8. https://doi.org/10.1038/s41592-021-01101-x.
47. Eddy SR. Accelerated profile HMM searches. PLoS Comput Biol. 2011;7:e1002195. https://doi.org/10.1371/journal.pcbi.1002195.
48. Mistry J, Chuguransky S, Williams L, Qureshi M, Salazar GA, Sonnhammer ELL, et al. Pfam: The protein families database in 2021. Nucleic Acids Res. 2021;49:D412–9. https://doi.org/10.1093/nar/gkaa913.
49. Manni M, Berkeley MR, Seppey M, Simão FA, Zdobnov EM. BUSCO update: novel and streamlined workflows along with broader and deeper phylogenetic coverage for scoring of eukaryotic, prokaryotic, and viral genomes. Mol Biol Evol. 2021;38:4647–54. https://doi.org/10.1093/molbev/msab199.
50. Patro R, Duggal G, Love MI, Irizarry RA, Kingsford C. Salmon provides fast and bias-aware quantification of transcript expression. Nat Methods. 2017;14:417–9. https://doi.org/10.1038/nmeth.4197.
51. Love MI, Huber W, Anders S. Moderated estimation of fold change and dispersion for RNA-seq data with DESeq2. Genome Biol. 2014;15:550. https://doi.org/10.1186/s13059-014-0550-8.
52. Langfelder P, Horvath S. WGCNA: an R package for weighted correlation network analysis. BMC Bioinformatics. 2008;9:559. https://doi.org/10.1186/1471-2105-9-559.

53. Shannon P, Markiel A, Ozier O, Baliga NS, Wang JT, Ramage D, et al. Cytoscape: a software environment for integrated models of biomolecular interaction networks. Genome Res. 2003;13:2498–504. https://doi.org/10.1101/gr.1239303.
54. Yu G, Wang LG, Han Y, He QY. clusterProfiler: an R package for comparing biological themes among gene clusters. OMICS. 2012;16:284–7. https://doi.org/10.1089/omi.2011.0118.
55. Yano M, Katayose Y, Ashikari M, Yamanouchi U, Monna L, Fuse T, et al. Hd1, a major photoperiod sensitivity quantitative trait locus in rice, is closely related to the Arabidopsis flowering time gene CONSTANS. Plant Cell. 2000;12:2473–83. https://doi.org/10.1105/tpc.12.12.2473.
56. Doi K, Izawa T, Fuse T, Yamanouchi U, Kubo T, Shimatani Z, et al. Ehd1, a B-type response regulator in rice, confers short-day promotion of flowering and controls FT-like gene expression independently of Hd1. Genes Dev. 2004;18:926–36. https://doi.org/10.1101/gad.1189604.
57. Xue W, Xing Y, Weng X, Zhao Y, Tang W, Wang L, et al. Natural variation in Ghd7 is an important regulator of heading date and yield potential in rice. Nat Genet. 2008;40:761–7. https://doi.org/10.1038/ng.143.
58. Komiya R, Ikegami A, Tamaki S, Yokoi S, Shimamoto K. Hd3a and RFT1 are essential for flowering in rice. Development. 2008;135:767–74. https://doi.org/10.1242/dev.008631.
59. Taoka KI, Ohki I, Tsuji H, Furuita K, Hayashi K, Yanase T, et al. 14-3-3 proteins act as intracellular receptors for rice Hd3a florigen. Nature. 2011;476:332–5. https://doi.org/10.1038/nature10272.
60. Shim JS, Jang G. Environmental signal-dependent regulation of flowering time in rice. Int J Mol Sci. 2020;21:6155. https://doi.org/10.3390/ijms21176155.
61. Katoh K, Standley DM. MAFFT multiple sequence alignment software version 7: improvements in performance and usability. Mol Biol Evol. 2013;30:772–80. https://doi.org/10.1093/molbev/mst010.
62. Capella-Gutiérrez S, Silla-Martínez JM, Gabaldón T. trimAl: a tool for automated alignment trimming in large-scale phylogenetic analyses. Bioinformatics. 2009;25:1972–3. https://doi.org/10.1093/bioinformatics/btp348.
63. Minh BQ, Schmidt HA, Chernomor O, Schrempf D, Woodhams MD, von Haeseler A, et al. IQ-TREE 2: new models and efficient methods for phylogenetic inference in the genomic era. Mol Biol Evol. 2020;37:1530–4. https://doi.org/10.1093/molbev/msaa015.
64. Lin SY, Shi WW, Miu BB, Ding YL. Research advances in reproduction biology of bamboos. World Bamboo Rattan. 2010;8:1–6. https://doi.org/10.13640/j.cnki.wbr.2010.02.006.
65. Long H, Chu CH, Jin DK, Lü Z, Wang SG. Anatomical observation and analysis on floral of Bambusa tuldoides. Guihaia. 2022;42:174–82. https://doi.org/10.11931/guihaia.gxzw202107024.
66. Niu ZY, Qin QM, Ni JB, Cai ZY, Tong YH, Xia NH. The floral morphology of Pseudosasa nanunica (Poaceae, Bambusoideae). PhytoKeys. 2026;271:83–92. https://doi.org/10.3897/phytokeys.271.183110.
67. Bommert P, Whipple C. Grass inflorescence architecture and meristem determinacy. Semin Cell Dev Biol. 2018;79:37–47. https://doi.org/10.1016/j.semcdb.2017.10.004.

68. Huang JQ, Huang HH, He FJ, Li ZJ, Pan CH, Li SQ. The formation of microspore and the development of male gametophyte of Phyllostachys praecox. J Bamboo Res. 1999;18:55–8.
69. Yao W, Li C, Lin S, Wang J, Fan T, Zhao W. The structures of floral organs and reproductive characteristics of an ornamental bamboo species, Pleioblastus pygmaeus. Hortic Plant J. 2023;9:589–601. https://doi.org/10.1016/j.hpj.2022.06.002.
70. Zhao WQ, Guo CC, Wang Y, Xiao J, Wu ZC, Liu HW, et al. Sporogenesis and gametogenesis of Pseudosasa viridula. Guihaia. 2022;42:143–51. https://doi.org/10.11931/guihaia.gxzw202010017.
71. Zhou L, Yan YD, Liu JX, Wang SS, Yang DJ, Wang SG. Study on the morphological structure and anther abortion of Phyllostachys nigra flowers. J Nanjing Univ Nat Sci Ed. 2025;49:210–6. https://doi.org/10.12302/j.issn.1000-2006.202308026.
72. Lin SY, Fu HJ, Wan YW, Zhang SX, Zhu RJ, Wang FS, et al. Anther development and floral morphology characteristics of Bambusa oldhami 'Xia Zao' ZSX. J Nanjing Univ Nat Sci Ed. 2019;43:7–13. https://doi.org/10.3969/j.issn.1000-2006.201711031.
73. Li XF, Lin XC, Shi Y, Guo XQ, Fang W. Flowering biological characteristics and pollen viability of Phyllostachys nigra. China Sci Technol. 2009;23:64–7.
74. Gopakumar B, Das MC, Shameena MK, Jero-Mathu A, Nath AJ, Das AK. Floral biology and pollen sterility in relation to seed set in Bambusa balcooa. J Trop Sci. 2017;29:504–8.
75. Mizuki I, Sato A, Matsuo A, Suyama Y, Suzuki JI, Makita A. Clonal structure, seed set, and self-pollination rate in mass-flowering bamboo species during off-year flowering events. PLoS ONE. 2014;9:e105051. https://doi.org/10.1371/journal.pone.0105051.
76. Chakraborty S, Biswas P, Dutta S, Basak M, Guha S, Chatterjee U, et al. Studies on reproductive development and breeding habit of the commercially important bamboo Bambusa tulda Roxb. Plants (Basel). 2021;10:2375. https://doi.org/10.3390/plants10112375.
77. Zhao JX, Wang S, Liu J, Jiang XD, Wen J, Suo ZQ, et al. A comparative full-length transcriptomic resource provides insight into the perennial monocarpic mass flowering. Plant J. 2023;116:1842–55. https://doi.org/10.1111/tpj.16452.
78. Louis B, Waikhom SD, Goyari S, Jose RC, Roy P, Talukdar NC. First proteome study of sporadic flowering in bamboo species (Bambusa vulgaris and Dendrocalamus manipureanus) reveal the boom is associated with stress and mobile genetic elements. Gene. 2015;574:255–64. https://doi.org/10.1016/j.gene.2015.08.010.
79. Zong W, Ren D, Huang M, Sun K, Feng J, Zhao J, et al. Strong photoperiod sensitivity is controlled by cooperation and competition among Hd1, Ghd7 and DTH8 in rice heading. New Phytol. 2021;229:1635–49. https://doi.org/10.1111/nph.16946.
80. Li C, Liu XJ, Yan Y, Alam MS, Liu Z, Yang ZK, et al. OsLHY is involved in regulating flowering through the Hd1- and Ehd1-mediated pathways in rice (Oryza sativa L). Plant Sci. 2022;315:111145. https://doi.org/10.1016/j.plantsci.2021.111145.
81. Cho LH, Yoon J, Tun W, Baek G, Peng X, Hong WJ, et al. Cytokinin increases vegetative growth period by suppressing florigen expression in rice and maize. Plant J. 2022;110:1619–35.

https://doi.org/10.1111/tpj.15760.

82. Giaume F, Bono GA, Martignago D, Miao Y, Vicentini G, Toriba T, et al. Two florigens and a florigen-like protein form a triple regulatory module at the shoot apical meristem to promote reproductive transitions in rice. Nat Plants. 2023;9:525–34. https://doi.org/10.1038/s41477-023-01383-3.
83. Wei S, Cheng L, Qian H, Li X, Shang L, Zhou Y, et al. Florigen-like protein OsFTL1 promotes flowering without essential florigens Hd3a and RFT1 in rice. J Integr Plant Biol. 2025;67:1307–22. https://doi.org/10.1111/jipb.13856.
84. Sun R, Ding Y, Mimura M, Nishide N, Izawa T. Temporal transcriptome analysis reveals the two-phase action of florigens in rice flowering. Theor Appl Genet. 2025;138:100. https://doi.org/10.1007/s00122-025-04869-0.
85. Verelst W, Twell D, de Folter S, Immink RGH, Saedler H, Münster T. MADS-complexes regulate transcriptome dynamics during pollen maturation. Genome Biol. 2007;8:R249. https://doi.org/10.1186/gb-2007-8-11-r249.
86. Adamczyk BJ, Fernandez DE. MIKC* MADS domain heterodimers are required for pollen maturation and tube growth in Arabidopsis. Plant Physiol. 2009;149:1713–23. https://doi.org/10.1104/pp.109.135806.
87. Wu F, Shi X, Lin X, Liu Y, Chong K, Theißen G, et al. The ABCs of flower development: mutational analysis of AP1/FUL-like genes in rice provides evidence for a homeotic (A)-function in grasses. Plant J. 2017;89:310–24. https://doi.org/10.1111/tpj.13386.
88. Zhang Y, Zhang J, Song M, Lin X, Tong Z, Ding M. Comprehensive analysis of five Phyllostachys edulis SQUA-like genes and their potential functions in flower development. Int J Mol Sci. 2021;22:10868. https://doi.org/10.3390/ijms221910868.
89. Nagasawa N, Miyoshi M, Sano Y, Satoh H, Hirano H, Sakai H, et al. SUPERWOMAN1 and DROOPING LEAF genes control floral organ identity in rice. Development. 2003;130:705–18. https://doi.org/10.1242/dev.00294.
90. Dreni L, Jacchia S, Fornara F, Fornari M, Ouwerkerk PBF, An G, et al. The D-lineage MADS-box gene OsMADS13 controls ovule identity in rice. Plant J. 2007;52:690–9. https://doi.org/10.1111/j.1365-313X.2007.03272.x.
91. Cui R, Han J, Zhao S, Su K, Wu F, Du X, et al. Functional conservation and diversification of class E floral homeotic genes in rice (Oryza sativa). Plant J. 2010;61:767–81. https://doi.org/10.1111/j.1365-313X.2009.04101.x.
92. Zhang Y, Tang D, Lin X, Ding M, Tong Z. Genome-wide identification of MADS-box family genes in moso bamboo (Phyllostachys edulis) and a functional analysis of PeMADS5 in flowering. BMC Plant Biol. 2018;18:176. https://doi.org/10.1186/s12870-018-1394-2.
93. Zhu Y, Wang S, Shu D, Huang W, Ouyang Z, Zheng S, et al. Comprehensive characterization of the PeMADS gene family in Phyllostachys edulis reveals new insights into floral development and evolution. Front Plant Sci. 2026;17:1806675. https://doi.org/10.3389/fpls.2026.1806675.

94. Zhang J, Xu GX, Xue HY, Hu J. Foundation and current progress of plant evolutionary developmental biology. Chin Bull Bot. 2007;24:1–30.
95. Liu Y, Guo C, Xu G, Shan H, Kong H. Evolutionary pattern of the regulatory network for flower development: insights gained from a comparison of two Arabidopsis species. J Syst Evol. 2011;49:528–38. https://doi.org/10.1111/j.1759-6831.2011.00158.x.

Figures

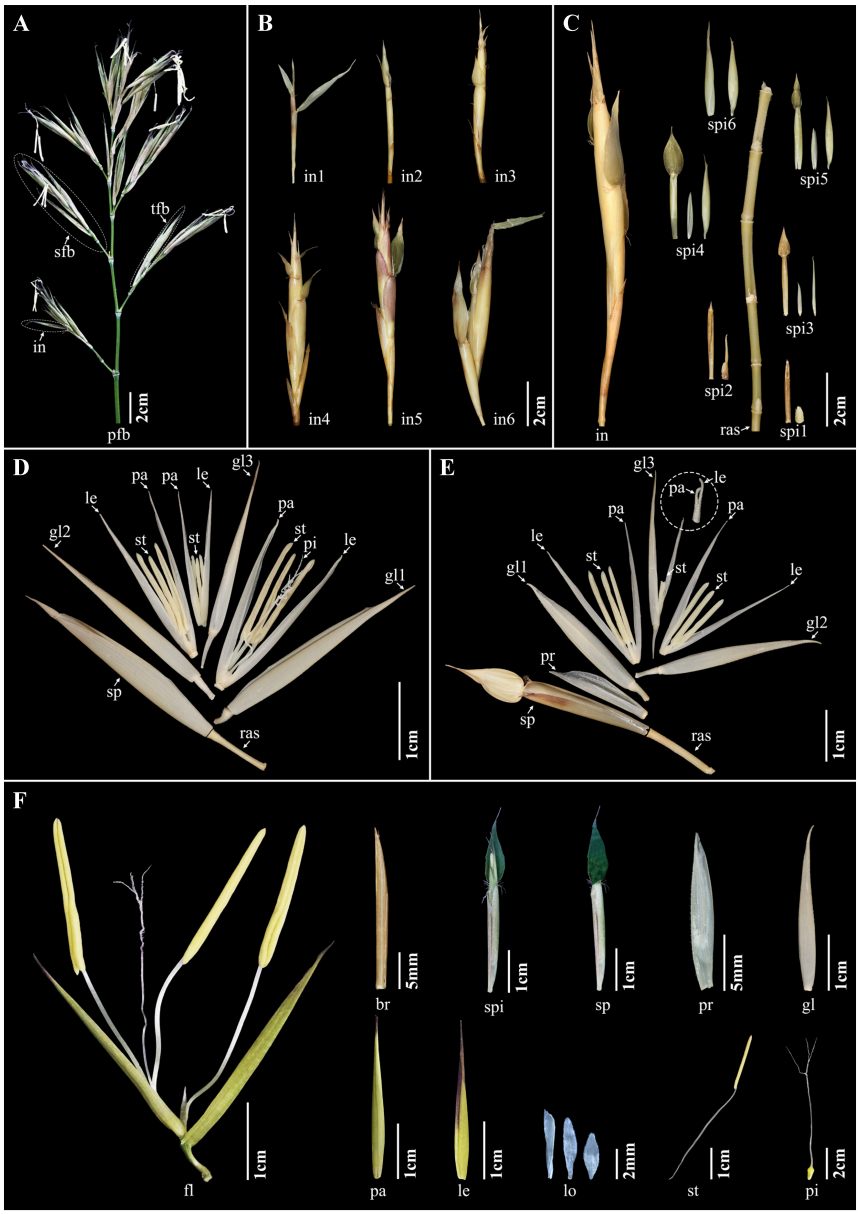


Figure 1

Anatomical structure of the inflorescence-spikelet-floret hierarchy in *Phyllostachys reticulata*. (A) Flowering branch; (B) inflorescence development; (C) hierarchical organization of the inflorescence; (D) structure of a terminal spikelet; (E) structure of a lateral spikelet; (F) anatomical structure of the inflorescence. Abbreviations: br, bract; fl, floret; gl, glume; in, inflorescence; in1-6, six developmental stages of the inflorescence; le, lemma; lo, lodicule; pa, palea; pi, pistil; pr, prophyll; pfb, primary flowering

branch; ras, inflorescence axis; sfb, secondary flowering branch; sp, spathe; spi, spikelet; spi1-6, spikelets numbered sequentially from the base to the apex within the same inflorescence; st, stamen; tfb, tertiary flowering branch.

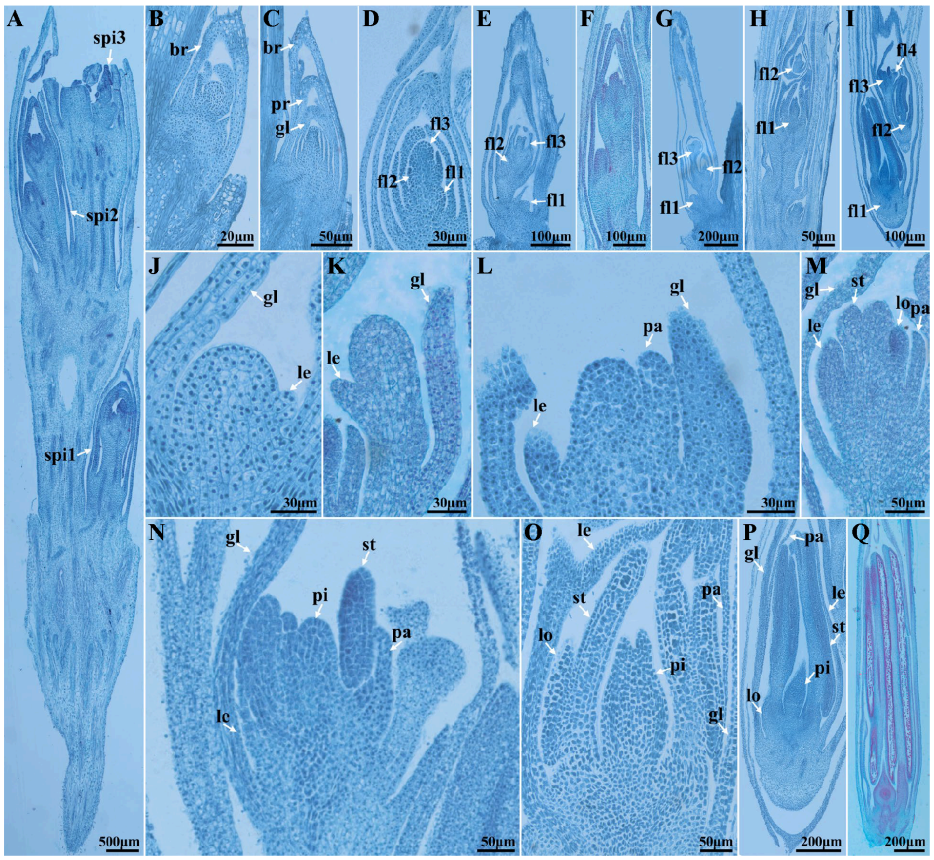


Figure 2

Initiation and development of spikelets and florets in *Phyllostachys reticulata*. (A) Longitudinal section of an inflorescence showing spikelets at different positions along the inflorescence axis; (B) spikelet primordium enclosed by a bract; (C) differentiation of the glume and prophyll primordia; (D-E) formation of floret primordia; (F-G) elongation of the spikelet-axis internodes and further floret development; (H-I) late stages of spikelet development, showing differences in developmental progression among florets at different positions within the same spikelet; (J) initiation of the lemma primordium; (K) lemma elongation; (L) initiation of the palea primordium; (M) initiation of the lodicule and stamen primordia; (N) differentiation of the stamen and pistil primordia; (O) further development of the floral organs; (P) floret at a late developmental stage; (Q) longitudinal section of a nearly mature floret. Abbreviations: br, bract; fl, floret; fl1-4, florets numbered sequentially from the base to the apex within the same spikelet; gl, glume; le, lemma; lo, lodicule; pa, palea; pi, pistil; pr, prophyll; spi, spikelet; spi1-3, spikelets numbered sequentially from the base to the apex within the same inflorescence; st, stamen. Scale bars are indicated in the panels.

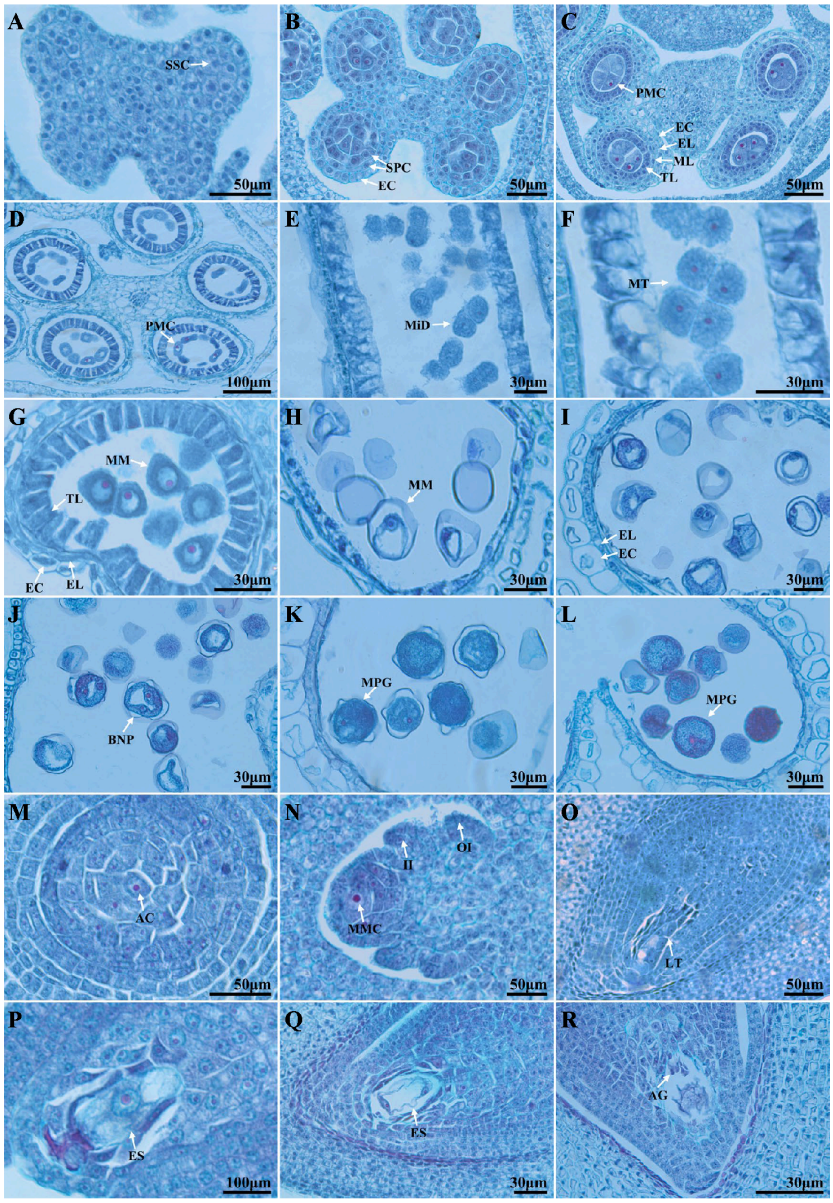


Figure 3

Microsporogenesis, megasporogenesis, and male and female gametophyte development in *Phyllostachys reticulata*. (1) Microsporogenesis and male gametophyte development (A-L). (A) Secondary sporogenous cells (SSCs); (B) two layers of secondary parietal cells (SPCs); (C) pollen mother cells (PMCs); (D) pollen mother cells undergoing meiosis; (E) microspore dyad (MiD); (F) microspore tetrad (MT); (G) mononucleate microspore (MM); (H) middle-to-late mononucleate microspore stage; (I-

J) formation of the vegetative and generative cells; (K) generative cell free within the vegetative-cell cytoplasm; (L) mature pollen grain (MPG). BNP, binucleate pollen; EC, epidermal cell; EL, endothecial layer; ML, middle layer; TL, tapetum. (2) Megasporogenesis and female gametophyte development (M-R). (M) Archesporial cell (AC); (N) megaspore mother cell (MMC); (O) linear megaspore tetrad (LT); (P) uninucleate embryo sac; (Q) binucleate embryo sac; (R) group of antipodal cells (AG). ES, embryo sac; II, inner integument; OI, outer integument.

A

Evaluation Index	Embryophyta odb10	Poales odb10
Total BUSCO Groups (n)	1,614	4,896
Complete BUSCOs (C)	91.1% (1,471)	92.6% (4,531)
Complete and single-copy BUSCOs (S)	68.1% (1,099)	61.9% (3,030)
Complete and duplicated BUSCOs (D)	23.0% (372)	30.7% (1,501)
Fragmented BUSCOs (F)	6.1% (99)	3.0% (149)
Missing BUSCOs (M)	2.8% (44)	4.4% (216)

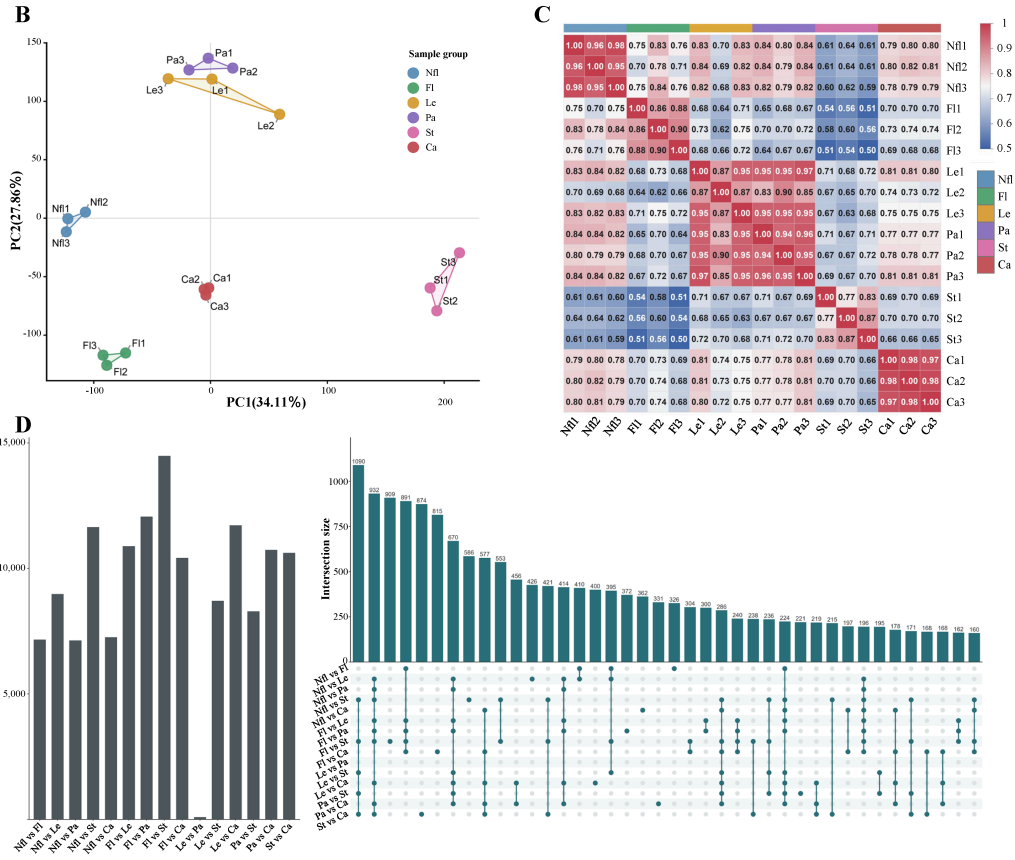


Figure 4

Completeness of the integrated transcriptome assembly and global expression patterns across six tissues of *Phyllostachys reticulata*. (A) BUSCO completeness assessment based on the Embryophyta odb10 and Poales odb10 datasets; (B) principal component analysis based on the 5,000 transcripts with the highest expression variance after $\log_2(\text{TPM} + 1)$ transformation; (C) heatmap of expression correlations among the 18 samples, with colors from blue to red indicating increasing correlation coefficients; (D) UpSet plot of differentially expressed transcripts identified from all pairwise comparisons among the six tissues, showing the 40 largest exact intersections at padj < 0.01 and $|\log_2 FC| \geq 4$. Abbreviations: Nfl, leaf from a non-flowering branch; Fl, leaf from a flowering branch; Le, lemma; Pa, palea; St, stamen; Ca, carpel.

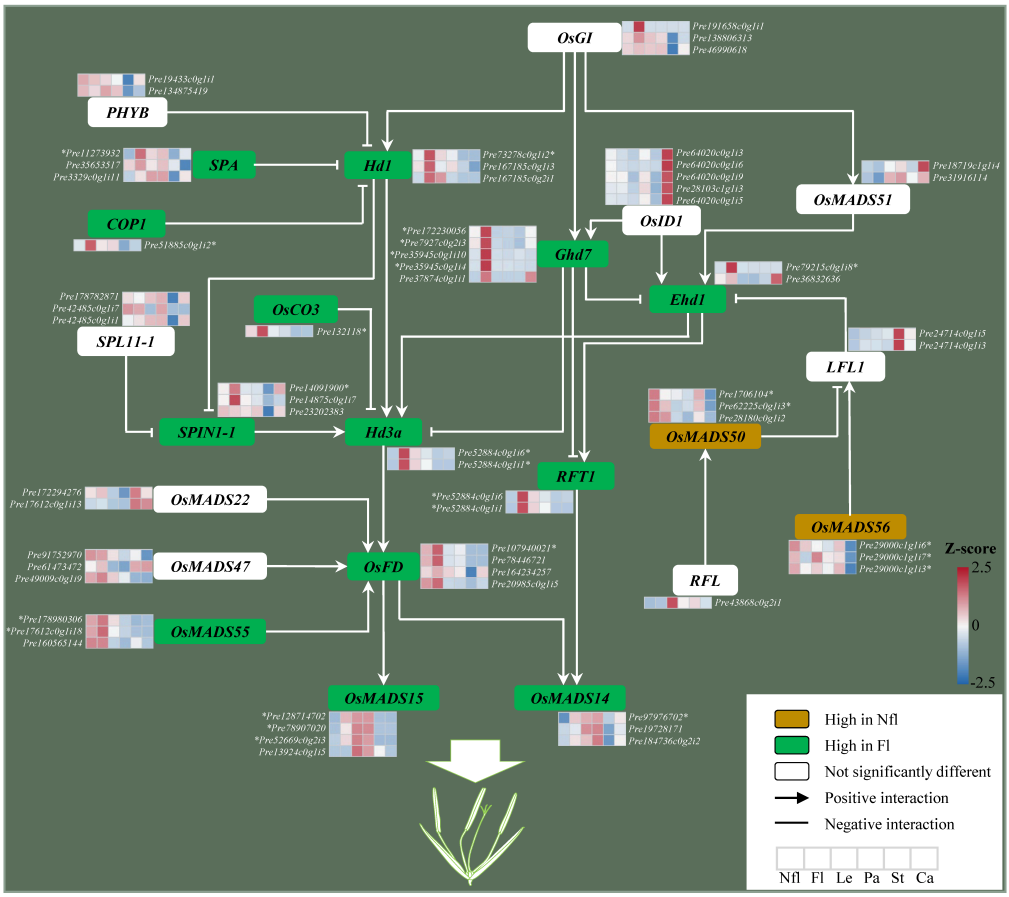


Figure 5

Putative photoperiodic flowering regulatory network in *Phyllostachys reticulata* and expression patterns of candidate homologous transcripts across six tissues. The network was constructed based on homology between *P. reticulata* and rice and flowering regulatory relationships previously reported in model plants, with nodes labelled using the corresponding rice reference gene names. Arrows and T-shaped bars indicate positive and negative regulation, respectively. Based on the direction of expression

differences between Nfl and Fl, green and ochre nodes indicate reference nodes whose corresponding *P. reticulata* candidate transcripts showed overall Fl-biased and Nfl-biased expression, respectively ($|\log_2 FC| \geq 1$), whereas white nodes indicate those that did not reach this fold-change threshold. Asterisks next to transcript IDs indicate individual transcripts that were significantly differentially expressed between Nfl and Fl. Heatmaps adjacent to the nodes show row-standardized expression levels (Z scores) of the candidate transcripts across the six tissues, with red and blue indicating relatively high and low expression, respectively. Abbreviations: Nfl, leaf from a non-flowering branch; Fl, leaf from a flowering branch; Le, lemma; Pa, palea; St, stamen; Ca, carpel.

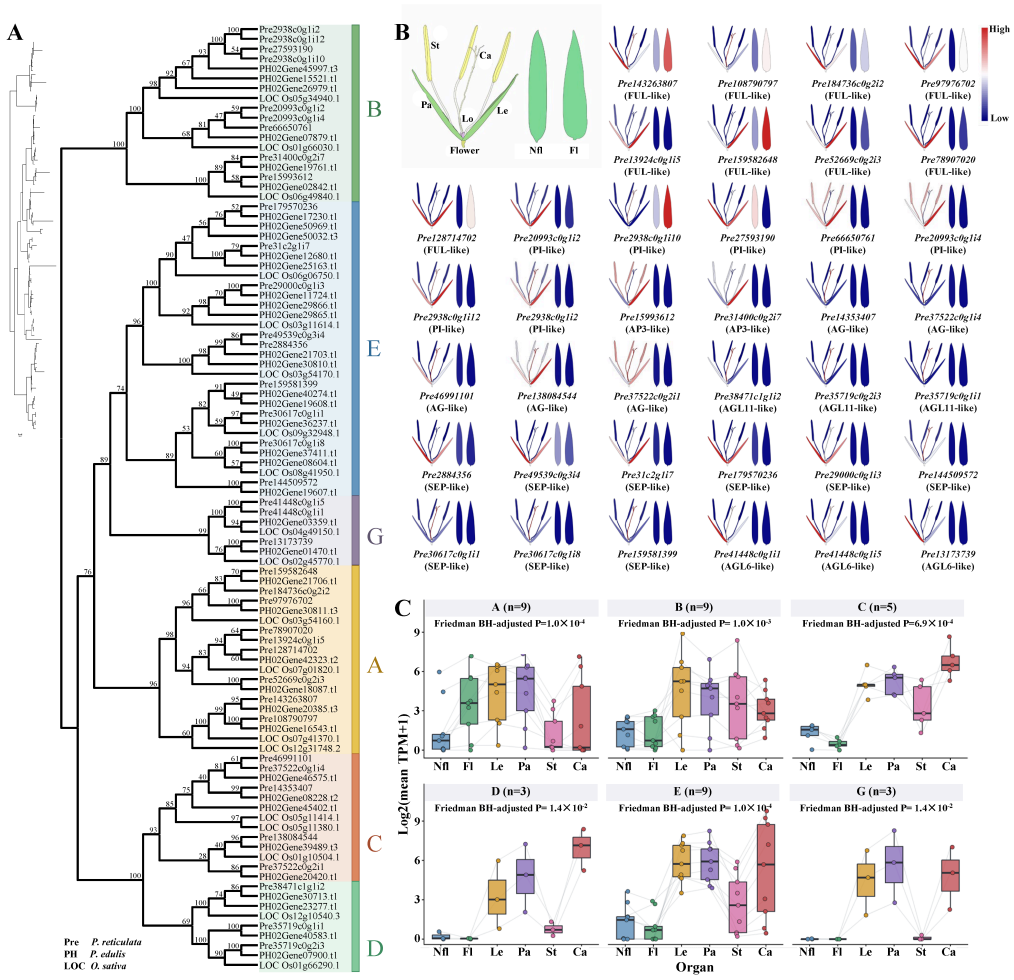


Figure 6

Phylogenetic classification and tissue-specific expression of ABCDEG-class MADS-box genes in *Phyllostachys reticulata*. (A) Phylogenetic tree constructed from MADS-box protein sequences of *P. reticulata*, *Phyllostachys edulis*, and rice. Sequences from *P. reticulata*, *P. edulis*, and rice are designated by the prefixes Pre, PH, and LOC, respectively. Differently colored branches and lightly shaded backgrounds indicate the A-, B-, C-, D-, E-, and G-class subfamilies. Values at the nodes indicate bootstrap support. (B)

Relative expression patterns of ABCDEG-class MADS-box genes in non-flowering leaves, flowering leaves, and different floral organs of *P. reticulata*. Red and blue indicate relatively high and low expression, respectively. (C) Expression distributions of A-, B-, C-, D-, E-, and G-class genes across the six tissues. Each point represents the mean expression of one gene across three biological replicates, and grey lines connect values for the same gene across tissues. Box plots show $\log_2$(mean TPM + 1). *P* values were obtained using the Friedman test and adjusted using the Benjamini-Hochberg procedure. Abbreviations: Nfl, leaf from a non-flowering branch; Fl, leaf from a flowering branch; Le, lemma; Pa, palea; St, stamen; Ca, carpel; Lo, lodicule.

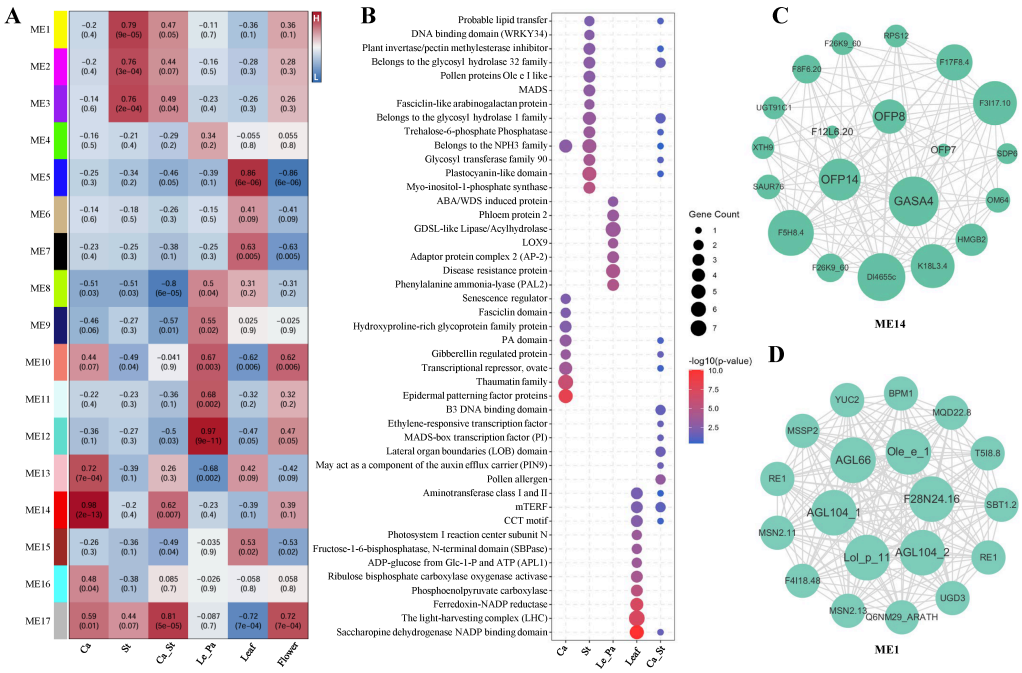


Figure 7

Organ-associated co-expression modules, functional enrichment, and candidate hub-gene networks in *Phyllostachys reticulata*. (A) Heatmap showing correlations between WGCNA module eigengenes and tissue traits. In each cell, the upper value represents the correlation coefficient and the value in parentheses below represents the *P*value; red and blue indicate positive and negative correlations, respectively. (B) Bubble plot of representative enriched functional terms in modules ME14, ME1, ME12,

ME17, and ME5. Bubble size represents the number of transcripts, and color indicates $-\log_{10}(P \text{ value})$. (C-D) Candidate hub-transcript co-expression networks of the red module (ME14) and yellow module (ME1), respectively. Node size represents network connectivity, and grey edges indicate co-expression relationships between transcripts. Abbreviations: Ca, carpel; St, stamen; Ca_St, combined carpel-stamen reproductive-organ trait; Le_Pa, combined lemma-palea trait.

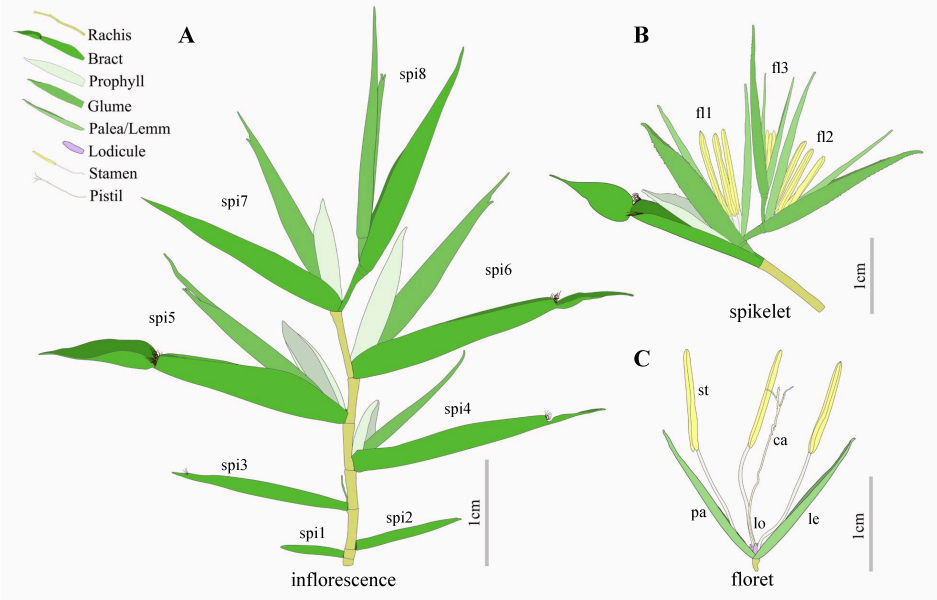


Figure 8

Schematic representation of the inflorescence, spikelet, and floret structures of *Phyllostachys reticulata*. (A) Overall inflorescence architecture, showing the rachis and the bracts and spikelets borne at successive nodes; (B) structure of a spikelet; (C) structure of a floret. Different colors indicate the rachis, bract, prophyll, glume, palea and lemma, lodicule, stamen, and pistil. Scale bars = 1 cm in all panels.

Supplementary Files

This is a list of supplementary files associated with this preprint. Click to download.

- Additionalfile1.zip
- Additionalfile2.zip